Article

Current Biology

Wake-active brainstem GABA neurons signal sleep pressure by upregulating AMPA receptors to drive recovery sleep

Graphical abstract

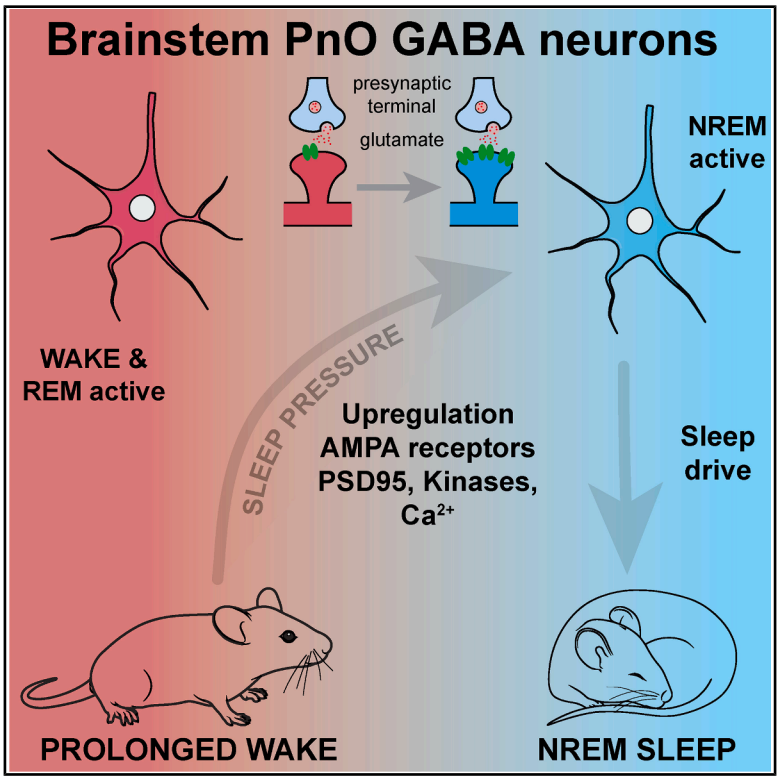

Highlights

- PnO GABA neurons switch from WAKE/REMS to NREMS after sleep loss
- Activating PnO GABA neurons prolongs NREMS and enhances rebound sleep
- Sleep deprivation increases GluA1 AMPA receptors in PnO GABA neurons
- Enhanced AMPA drive onto PnO GABA neurons implements sleep homeostasis

Authors

Wei Ba, Edward C. Harding, Mathieu Nollet, ..., Michael J. Courtney, William Wisden, Nicholas P. Franks

Correspondence

w.wisden@imperial.ac.uk (W.W.), n.franks@imperial.ac.uk (N.P.F.)

In brief

Ba et al. identify a WAKE/REMS-active GABAergic population in the pontine oral nucleus that senses sleep pressure. After sleep deprivation, these neurons switch to NREMS, upregulate GluA1-containing AMPA receptors, and drive rebound sleep, revealing a synaptic-plasticity mechanism for homeostatic sleep recovery.

Ba et al., 2026, Current Biology *36*, 2823–2839
June 8, 2026
https://doi.org/10.1016/j.cub.2026.04.059

CellPress

Current Biology

CellPress
OPEN ACCESS

Article

Wake-active brainstem GABA neurons signal sleep pressure by upregulating AMPA receptors to drive recovery sleep

Wei Ba,[1,9] Edward C. Harding,[1,9,10] Mathieu Nollet,[1,2,9] Kyoko Tossell,[1] Li-Li Li,[3,4] Sara Wong,[1] Berta Anuncibay Soto,[1,2] Raquel Yustos,[1] Li Li,[1,5] Jagoda Ostaszewska,[1] Hanns Ulrich Zeilhofer,[6,7] Alexei L. Vyssotski,[8] Michael J. Courtney,[3,4] William Wisden,[1,2,*] and Nicholas P. Franks[1,2,11,*]

[1]Department of Life Sciences, Imperial College London, London SW7 2AZ, UK
[2]UK Dementia Research Institute, Imperial College London, London SW7 2AZ, UK
[3]Neuronal Signalling Laboratory and Turku Screening Unit, Turku Bioscience Centre, University of Turku, 20520 Turku, Finland
[4]Turku Brain and Mind Center, University of Turku, 20014 Turku, Finland
[5]Department of Physiology, Hubei University of Chinese Medicine, Wuhan 430065, China
[6]Institute of Pharmacology and Toxicology, University of Zürich, Winterthurerstrasse 190, 8057 Zürich, Switzerland
[7]Institute of Pharmaceutical Sciences, Swiss Federal Institute of Technology (ETH) Zürich, Vladimir Prelog Weg 4, 8093 Zürich, Switzerland
[8]Institute of Neuroinformatics, University of Zürich and Swiss Federal Institute of Technology (ETH) Zürich, Winterthurerstrasse 190, 8057 Zürich, Switzerland
[9]These authors contributed equally
[10]Present address: Department of Pharmacology, University of Cambridge, Cambridge CB2 1QR, UK
[11]Lead contact
*Correspondence: w.wisden@imperial.ac.uk (W.W.), n.franks@imperial.ac.uk (N.P.F.)
https://doi.org/10.1016/j.cub.2026.04.059

SUMMARY

How the brain compensates for sleep deprivation (SD) by generating recovery sleep (RS) is not understood. Using Ca^{2+} photometry, we identified a WAKE/rapid eye movement sleep (REMS)-active somatostatin/parvalbumin GABAergic population in the mouse brainstem oral pontine reticular nucleus (PnO^{Vgat}). Following SD, PnO^{Vgat} cells transiently switched for the first hour to higher activity during non-REMS (NREMS), promoting RS. Chemogenetic activation of PnO^{Vgat} neurons prolonged NREMS, whereas ablation blunted electroencephalogram (EEG) delta power rebound and slowed RS accumulation. During RS, the selective switch of PnO^{Vgat} cells to having higher Ca^{2+} levels in NREMS correlated with elevated levels of synaptic proteins PSD95, activated calmodulin-dependent kinase II CaMKII (pCaMKII T286), activated PKA (pPKA T197), and GluA1-containing AMPA receptor subunits with enhanced serine phosphorylation. All increases started during SD and persisted after the first hour of RS. Patch-clamp recordings demonstrated increased postsynaptic AMPA/sleep homeostasis (NMDA) receptor ratios in PnO^{Vgat} cells 1 h after RS, indicating increased excitability and greater capacity to drive RS. In contrast, an intermingled population of GABA/glycinergic neurons did not respond to SD, despite having similar baseline WAKE/REMS activities and an ability to promote NREMS. The PnO also contained an intermingled population of excitatory PnO^{Vglut2} WAKE/REMS-active neurons; lesioning them caused hypoactivity, but sleep or WAKE amounts were unaffected. The synaptic homeostasis hypothesis (SHY) proposes that as wakefulness progresses, synaptic AMPA receptor activity is enhanced, and subsequently downregulated during NREMS to rebalance circuit function. We suggest that a variation of SHY implements catching up on lost sleep, with glutamate receptor plasticity in the PnO tracking time awake and adjusting NREMS amounts accordingly.

INTRODUCTION

Both stages of mammalian sleep, non-rapid eye movement sleep (NREMS) and rapid eye movement sleep (REMS), are regulated by homeostatic mechanisms—the longer wakefulness persists, the stronger the urge to sleep becomes, and there is usually then some catching up on lost sleep.[1,2] Although classically, the sleep drive is framed as being determined by two distinct processes, process S (homeostatic) and process C (circadian),[3] this concept of dual drives has recently been suggested to require refinement,[2] and it has been questioned whether the increase in electroencephalogram (EEG) delta (0.5–4 Hz) power after sleep deprivation (SD) is the best or only measure for sleep need.[1,2] Following SD, there is a recovery sleep (RS) NREMS, in which there is an immediate but short-lasting increase in the delta component of the EEG, and a slower, and probably more consequential, actual catching up of some of the lost NREMS, which takes place over the subsequent 48 h or so after SD.[1,2] How the brain detects sleep loss and then repays this sleep debt remains a central and unsolved

question, especially because the need to catch up on lost sleep suggests there is an important function for sleep.[1] Understanding what is being measured or tracked with wakefulness may reveal this function.

While fruit flies seem to have dedicated "sleep homeostasis" neurons,[4] it is unclear whether this is the case in vertebrates, in which neurons that promote sleep also sense sleep pressure, with possibly no particular dedicated homeostasis circuit. Sleep need, at least as inferred from the appearance of EEG delta waves, can be sensed locally in, for example, the neocortex.[5] In vertebrates, various circuits and cell types regulate catching up on sleep and are distributed throughout the brain: somatostatin/GABA cells in the prefrontal cortex,[6] neocortical pyramidal/dentate granule cells,[7] parvalbumin cells in neocortex,[8] galanin cells in the preoptic hypothalamus,[9–11] GABA cells in the ventral tegmental area (VTA),[12] serotonin cells in the dorsal raphe,[13] and thalamic nucleus reuniens and zona incerta neurons[14] all contribute to catching up on lost sleep after SD. After SD, some of these circuits produce both the transient increase in delta power and the partial catching up on lost sleep. In any case, the question is: what activates these diverse circuits to induce sleep pressure? In other words, what induces the sleep-promoting neurons to start firing?

During WAKE and sleep periods, some synapses physically change size, increasing and decreasing, change their composition, change their strength, or even disappear depending on synapse type and brain area,[15–18] and one function of NREMS could be to rebalance synaptic strength.[19,20] This is known as the synaptic homeostasis hypothesis (SHY). The essence of SHY is that during wakefulness, neocortical and hippocampal neurons acquire higher levels of excitatory ionotropic glutamate/AMPA receptors, as measured by more GluA1 AMPA receptor subunits during wakefulness than sleep, and more PKA- and calmodulin-dependent kinase II (CaMKII)-dependent phosphorylation on critical serines in the intracellular domains of GluA1, which produces more excitability.[21,22] These levels are reset during just a few hours of NREMS.[22] In forebrain synapses, the weakening of connections during sleep is produced by the Homer1a protein.[23] However, these findings do not indicate what the sleep drive itself is and how RS would be initiated in response to lost sleep.

An intriguing idea is that sleep pressure itself arises from synaptic plasticity. In this model, a longer time awake leads to more strengthening of synapses between sleep pressure-sensing cells and sleep-promoting cells.[24] In particular, studies in *Drosophila* have suggested that sleep loss induces synaptic modifications and increases synaptic strength via presynaptic N-methyl-D-aspartate (NMDA) glutamate receptor-dependent plasticity within the ellipsoid body of the fly brain, so that the sleep drive is a strengthening of communication between those neurons sensing sleep pressure and those that command sleep.[24] On the other hand, when we tested this idea in mice, we found that selectively ablating NMDA glutamate receptors from hypothalamic preoptic sleep-promoting galanin neurons left sleep homeostasis (as defined by the delta power increase) unaffected.[25] Nevertheless, a non-NMDA receptor mechanism for inducing RS was recently described in which SD in mice caused a presynaptic CaMKII-dependent increase in presynaptic arborization, in other words, a structural change, thereby enhancing synaptic coupling between thalamic reuniens and NREMS-inducing zona incerta neurons.[14] This change was associated with an increase in EEG delta power after SD and more consolidated NREMS.[14] Similarly, artificially increasing postsynaptic synapse sizes on spines of excitatory pyramidal cells in the prefrontal cortex increases EEG delta power and induces more NREMS.[26] Thus, the principle of plasticity as a way of encoding sleep drive could apply to various circuits, even if individual mechanisms are different.

Here, we investigated circuitry governing sleep-wake and, in particular, NREMS homeostasis circuitry in the brainstem, in a small region known as the oral pontine reticular nucleus (PnO), a likely component of the ascending reticular activating system. Work predating modern circuitry mapping techniques found that in cats and rats, injecting excitatory and inhibitory transmitter agonists and antagonists into the PnO affects amounts of REMS and WAKE.[27–32] One study of the PnO using modern methods showed that dual inhibitory glycinergic/GABAergic neurons in the mouse PnO (and neighboring caudal pontine reticular nucleus) project to the midline thalamus, and, when opto-activated, lead to behavioral arrest—all behaviors of the mice became suspended, but the mice maintained their posture[33]; concomitantly, large amplitude slow oscillations in the delta frequency range of local field potentials in the neocortex were induced.[33]

By surveying three PnO neuronal classes, WAKE-promoting glutamatergic, and NREMS-promoting glycinergic and GABAergic cells, we discovered that the somatostatin/parvalbumin-expressing GABAergic neurons, but not glycinergic or glutamatergic neurons, regulate sleep homeostatic responses—the GABAergic cells switch their activity, as inferred from Ca^{2+} levels, from WAKE- and REMS-active to NREMS-active, to drive RS. Lesioning them eliminates the increase in EEG delta power following SD and slows the rate of subsequent recovery NREMS. To our knowledge, this study is the first to report a defined neuronal population altering its spontaneous sleep-wake activity profile in response to extended wakefulness. We find that the mechanism for how the initial part of this process is likely implemented, with an upregulation of synaptic scaffold proteins, kinases, and GluA1 AMPA receptors, highly resembles that proposed for SHY.

RESULTS

In baseline conditions, all GABAergic, glycinergic, and glutamatergic populations in the PnO have their highest calcium activities in WAKE and REMS

We began by examining the natural dynamics of the PnO neurons, as assessed by their internal Ca^{2+} levels, across the sleep-wake cycle. *AAV-DIO-GCaMP6s* was injected into the PnO of *Vgat-Cre*, *GlyT2-Cre*, and *Vglut2-Cre* mice (Figures 1 and S1), and neuronal population activity was measured by photometry (Figure 1A). In PnO^{Vgat} neurons, higher Ca^{2+} levels were present during WAKE and REMS, whereas levels during NREMS were lower (Figure 1B). The signals increased when mice transitioned from NREMS to REMS or to WAKE. A time-locked decrease in activity of PnO^{Vgat} neurons occurred at WAKE-NREMS transitions (Figures 1C and 1D). PnO^{GlyT2} neurons exhibited similar patterns of spontaneous Ca^{2+} levels (Figures S1A and S1B), with the highest Ca^{2+} transients during

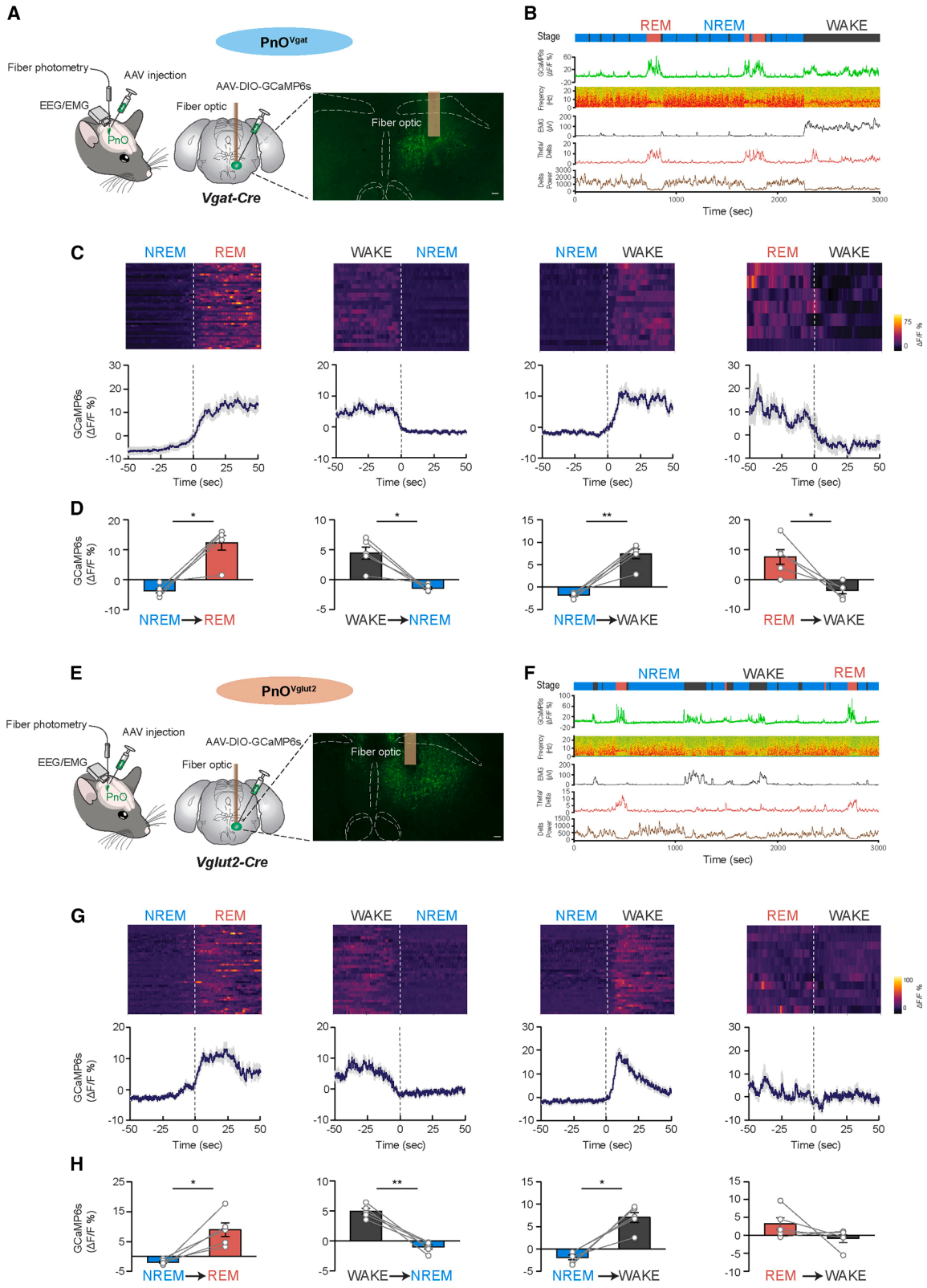

(legend on next page)

REMS, followed by WAKE, and the lowest activity during NREMS (Figure S1C). PnO^{Vglut2} neurons had the highest Ca^{2+} during WAKE, followed by REMS and NREMS (Figures 1E and 1F), with the Ca^{2+} transients peaking soon after the NREMS-WAKE transitions and then decaying (Figures 1G and 1H). Thus, both inhibitory and excitatory neurons in the PnO, regardless of their transmitter usage, are predominantly WAKE- and REMS-active.

Inhibitory PnO neurons produce NREMS, whereas glutamatergic neurons maintain locomotor activity

We next evaluated how PnO neuronal activity influenced sleep-wake states (Figures 2, S2, and S3). By bilateral AAV injections (Figure 2A), we expressed the excitatory chemogenetic *hM3Dq-mCherry* receptor selectively in *Vgat*, *GlyT2*, and *Vglut2* PnO neurons of the respective *Cre* mice. Sleep and WAKE were then monitored after clozapine N-oxide (CNO, 0.3 mg/kg intraperitoneal [i.p.]) injections. Surprisingly, given their selective WAKE- and REMS-active Ca^{2+} profile, chemo-activating PnO^{Vgat} neurons induced NREMS for 3 h following CNO injection during the dark phase, a period when mice are more likely to be active (Figures 2B–2D). Total duration of WAKE was significantly reduced, whereas REMS remained unaffected. Consistently, the latency to NREMS was shortened following CNO injection, compared with the control saline-injected mice (Figure 2E). The increased NREMS duration was due to longer sleep bouts, suggesting consolidated NREMS (Figures 2F and 2G). Similarly, chemo-activation of the PnO^{Vgat} neurons during the light (inactive) period increased the duration of NREMS for 4 h at the expense of both WAKE and REMS (Figures S2A and S2B). No change was found in the control mice injected with *AAV-DIO-mCherry* (Figures S2C and S2D). We next chemogenetically tested the other inhibitory population, PnO^{GlyT2}. Similarly, and surprisingly, given their REMS preference deduced from Ca^{2+} levels, PnO^{GlyT2} neurons also produced NREMS when activatyed chemogenetically, which lasted for 2 h (Figures S3A–S3E). For both PnO^{Vgat} and PnO^{GlyT2} neurons, REMS was postponed during CNO activation. In contrast, after chemo-activating PnO^{Vglut2} neurons during the light (inactive) period, prolonged WAKE (lasting up to 6 h) occurred at the expense of both NREMS and REMS (Figures 2H–2K). The latencies to both NREMS and REMS were significantly increased (Figure 2L). Bout lengths and bout counts are shown in Figures 2M and 2N, respectively.

Thus, inhibitory PnO neurons can strongly produce NREMS while postponing REMS episodes, but there is an intriguing disconnect with the Ca^{2+} photometry data for these cells, in which the highest Ca^{2+} levels were during WAKE and REMS. In contrast, PnO^{Vglut2} neurons can generate extended WAKE, and this does correlate with their Ca^{2+} activity in baseline conditions. To look more closely at the identities of PnO^{Vgat} neurons, *AAV-DIO-GFP* was injected into the PnO area of *Vgat-Cre* mice, acute brain slices were prepared, and GFP-expressing cells were analyzed by single-cell reverse transcription quantitative PCR (RT-qPCR) (Figure S3F). GlyT2 cells in the PnO are expected to be a subset of the total *Vgat*-expressing population, and about 20% of the *Vgat-Cre* PnO^{Vgat} cells contained *GlyT2* transcripts (Figure S3F). These cells may be some of the dual glycine/GABA cells that produce behavioral arrest when activated.[33] Many (about 70%) of the *Vgat-Cre* PnO^{Vgat} neurons contained *somatostatin* (*Sst*) and *parvalbumin* (*Pvalb*) transcripts; a small number of PnO^{Vgat} cells also contained *Vglut2* transcripts. This substantial heterogeneity may contribute to regulating sleep.

Expression of the *hM3Dq-mCherry* receptor provided an opportunity to map the projections of PnO^{VGlut2} and PnO^{Vgat} neurons. Each type had a distinct pattern of ascending projections: mCherry-positive axons of PnO^{Vgat} neurons went primarily to the basal forebrain, ventral striatum, lateral hypothalamus (LH), zona incerta, and in the brain stem, the ventral area of the gigantocellular reticular nucleus (GRN) (Figure 3A); PnO^{Vglut2} neurons sent a different pattern of ascending projections, including to thalamic midline nuclei, the VTA, and dorsal GRN (Figure 3B).

We tested the necessity of the PnO cells in sleep regulation by using caspase-mediated selective lesioning (CASP). *AAV-DIO-CASP3* was bilaterally injected into the PnO of *Vgat-Cre* or *Vglut2*-Cre mice to generate PnO$^{Vgat\text{-}CASP}$ and PnO$^{Vglut2\text{-}CASP}$ mice, respectively. In each case, CASP mice were paired with their littermate controls injected with *AAV-DIO-mCherry* (PnO$^{Vgat\text{-}mCherry}$ and PnO$^{Vglut2\text{-}mCherry}$ controls) (Figure 4A). The majority of PnO neurons were ablated 4 weeks after the viral injection (85% PnO^{Vgat} and 93% PnO^{Vglut2} were eliminated, respectively) (Figure S4). In PnO$^{Vgat\text{-}CASP}$ mice, there was

Figure 1. Spontaneous activity of PnO neurons across sleep-wake states

(A–D) PnO^{Vgat} neuronal population activities recorded using fiber photometry with EEG/EMG recordings in freely behaving *Vgat-Cre* mice.

(A) Left, illustration of the experimental setup. Right, image with higher magnification showing the location of *AAV-DIO-GCaMP6s* expressing neurons and a fiber optic for capturing spontaneous activities of PnO^{Vgat} neurons. Scale bars, 100 μm.

(B) Representative fiber photometry recordings aligned with EEG/EMG signals of the PnO^{Vgat} neurons.

(C) Combined fluorescence responses during transitions between vigilance states for all mice. Top, individual traces with color-coded fluorescence intensity. Bottom, mean responses of each transition (black line) ± SEM (gray).

(D) Quantification of PnO population activities during sleep-wake transitions. Error bars represent SEMs. Individual circles in the graphs indicate independent mice used per experiment.

(E–H) Spontaneous activities of the PnO^{Vglut2} neurons across sleep-wake cycles combining fiber photometry with EEG/EMG recordings in freely behaving *Vglut2-Cre* mice.

(E) Left, illustration of the experimental setup. Right, image with higher magnification showing the location of *AAV-DIO-GCaMP6s* expressing neurons and a fiber optic for capturing spontaneous activities of PnO^{Vglut2} neurons. Scale bars, 100 μm.

(F) Representative fiber photometry recordings aligned with EEG/EMG signals of the PnO^{Vglut2} neurons.

(G) Combined fluorescence responses during transitions between vigilance states for all mice. Top, individual traces with color-coded fluorescence intensity. Bottom, mean responses of each transition (black line) ± SEM (gray).

(H) Quantification of PnO population activities during sleep-wake transitions. Individual circles in the graphs indicate independent mice used per experiment. Error bars represent SEMs. Individual circles in the graphs indicate independent mice used per experiment.*$p < 0.05$ and **$p < 0.01$, paired *t* test.

See also Figure S1.

CellPress
OPEN ACCESS

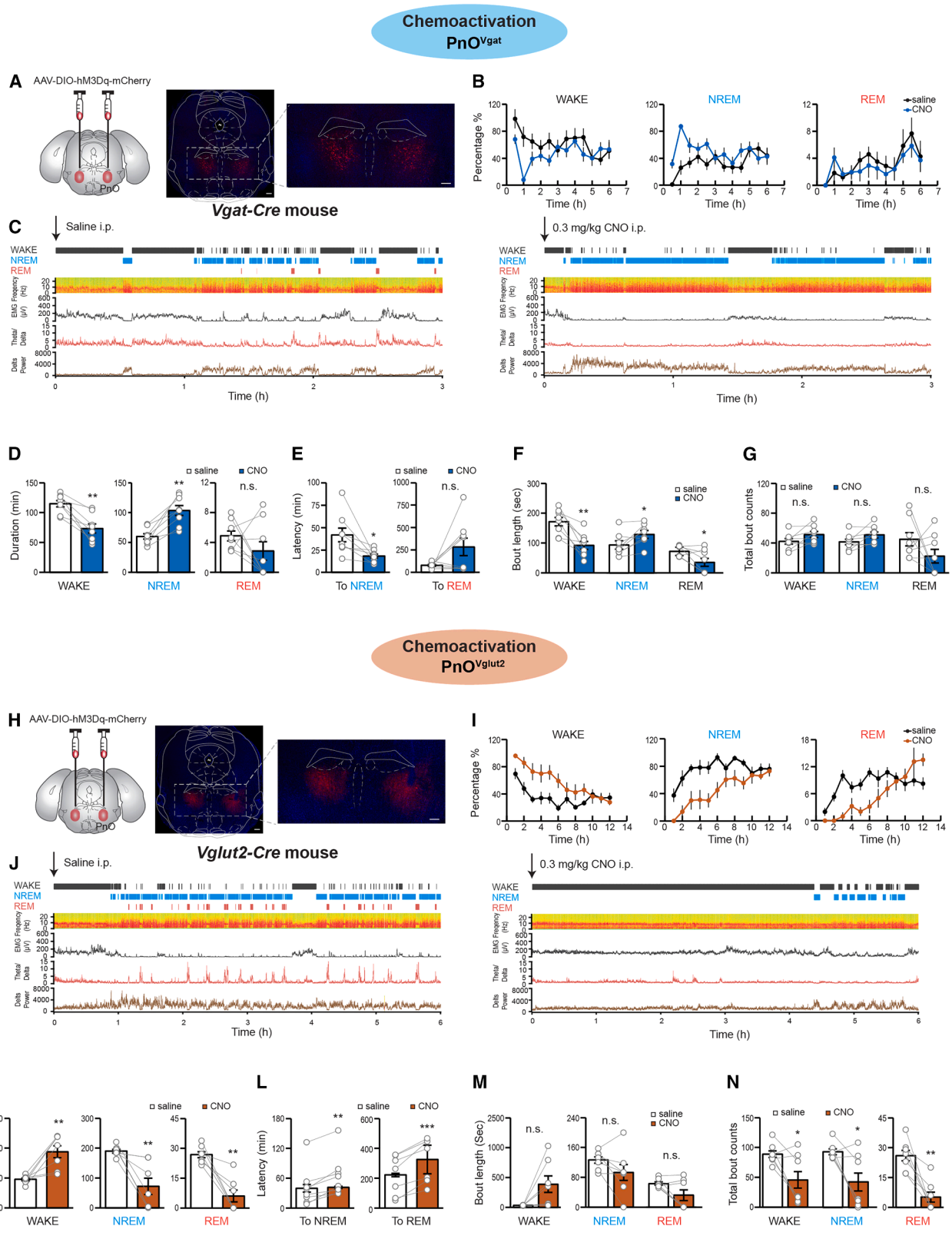

(legend on next page)

significantly shortened NREMS in both light and dark periods, due to fewer NREMS bouts; conversely, the duration of wakefulness was increased, whereas REMS remained unaffected (Figures 4B–4E). For the sleep-wake microarchitecture, ablating PnO^{Vgat} neurons reduced the transitions between WAKE and NREMS by about 20% in both light and dark phases (Figure 4F). Consistently, $PnO^{Vgat\text{-}CASP}$ mice traveled longer distances in the open-field assay compared with control $PnO^{Vgat\text{-}mCherry}$ mice (Figure 4G).

In $PnO^{Vglut2\text{-}CASP}$ mice, no changes in baseline sleep were detected when compared to the $PnO^{VGlut2\text{-}mCherry}$ control animals (Figures 4H–4J). However, compared with controls, $PnO^{Vglut2\text{-}CASP}$ mice were hypoactive, with a reduced travel distance in the open-field assay, suggesting that these mice spent more time in a quiet wakefulness state (Figure 4K).

These findings show that PnO^{Vgat} neurons are necessary for maintaining normal sleep structure (typical amounts of sleep), whereas PnO^{Vglut2} neurons support locomotion.

PnO^{Vgat} but not PnO^{GlyT2} neurons respond to sleep pressure and contribute to sleep homeostasis

We examined, by fiber photometry, whether PnO^{Vgat} or PnO^{GlyT2} neurons respond to high sleep pressure. 5 h of SD were performed by introducing novel objects, and GCaMP6s signals in the low (control) and high (SD) sleep pressure groups were then compared at the same circadian time (Figure 5A). Following 5 h of SD, the Ca^{2+} transients in the PnO^{Vgat} neurons were significantly increased during the first hour of recovery NREMS relative to those during the baseline NREMS (Figure 5B). An increased spike rate (spikes/min) was detected in the PnO^{Vgat} SD group during the first hour of RS, indicating that the PnO^{Vgat} neurons are highly sensitive to sleep need (Figure 5B). This elevated rate of Ca^{2+} spikes gradually decreased over time and returned to baseline levels by the third hour post-SD. These observations suggest that the increase in activity of PnO^{Vgat} neurons is reversible and coincides with the rise in delta power following SD (Figure 5B). In contrast, no difference in WAKE spike rate was observed after SD (Figure S5A). We performed the same experiment on PnO^{GlyT2} neurons (Figure 5C). Although exhibiting similar REMS/WAKE Ca^{2+} activity patterns and NREMS-promoting effects as PnO^{Vgat} cells under baseline conditions (Figures S3A–S3E), PnO^{GlyT2} neurons had low Ca^{2+} activity during RS, so did not respond to elevated sleep pressure (Figure 5C). Similarly, no change in the Ca^{2+} transients occurred in PnO^{VGlut2} neurons during recovery sleep compared with baseline sleep (Figures S5B and S5C). These results suggest that the state-switching property upon elevated sleep pressure, firing during WAKE and REMS, and then switching to activity during NREMS, is unique to PnO^{Vgat} neurons.

Using the $PnO^{Vgat\text{-}CASP}$ mice (with chronically deleted PnO^{Vgat} cells), we examined whether these neurons are required for homeostatic sleep regulation. Transiently increased EEG power of the delta band (0.5–4 Hz) marks the initial stages of recovery sleep.[2] As expected, this increased delta power was observed during the first 2 h of rRS in $PnO^{Vgat\text{-}mCherry}$ control animals (Figure 5D). This increase became undetectable after 2 h, indicating that this feature of RS was dissipated (Figure S6). In control mice, the accumulated sleep loss resulting from 5 h of SD was fully recovered after 19 h of RS (Figure 5D). However, the immediate increase in delta power was absent in the $PnO^{Vgat-CASP}$ mice, and the rate of accumulation was less, with only 53% of the sleep loss recovered in the subsequent 19 h of RS (Figure 5D). These data suggest that PnO^{Vgat} neurons switch to an NREMS-active state upon high sleep need and are required for full homeostatic sleep regulation.

PnO^{Vgat} neurons upregulate synaptic scaffold proteins, serine kinases, and GluA1-containing AMPA glutamate receptors in response to elevated sleep pressure

Enhanced neuronal activity could result from increased excitatory synaptic input onto the PnO^{Vgat} neurons. We examined a possible underlying molecular mechanism that activates PnO^{Vgat} neurons in response to sleep need, focusing on the ionotropic AMPA-type glutamate receptors since they are major determinants of synaptic strength.[34] Mice were assigned into three groups: control (undisturbed sleep), SD (5 h), and RS (1 h of RS following 5 h of SD) (Figure 6A). Following this, the PnO region was micro-dissected from all three groups for the preparation to isolate synaptoneurosomes, a subcellular fractionation containing both the pre- and postsynaptic

Figure 2. PnO GABAergic neurons promote sleep, whereas PnO glutamatergic neurons induce wakefulness

(A–G) Chemogenetic activation of PnO^{Vgat} neurons induces sleep.

(A) Schematic illustrating excitation of PnO^{Vgat} neurons using DREADD receptors. *AAV-DIO-hM3Dq-mCherry* was injected into the PnO of *Vgat-Cre* mice. Immunostaining confirmed the expression of hM3Dq-mCherry in the PnO. Scale bars, 200 μm.

(B) 6-h sleep recordings post-saline (black) or CNO (blue) administration.

(C) Representative EEG/EMG recording post-saline or CNO (0.3 mg/kg) injections.

(D–E) Summarized changes of sleep duration (D) and latency (E) during the 3-h period post-injection.

(F) Average bout length in all vigilance states during 3 h of sleep recordings post-saline or CNO injection.

(G) Total bout counts in all vigilance states during 6 h of sleep recordings post-saline or CNO injection.

(H–N) Chemogenetic activation of PnO^{Vglut2} neurons induces wakefulness.

(H) Schematic illustrating excitation of PnO^{Vglut2} neurons using DREADD receptors. *AAV-DIO-hM3Dq-mCherry* was injected into the PnO of *Vglut2-Cre* mice. Immunostaining confirmed the expression of hM3Dq-mCherry in the PnO. Scale bars, 200 μm.

(I) Average percentage of WAKE, NREMS, and REMS states during 12-h sleep recordings post-saline (black) or CNO (orange) administration.

(J) Representative EEG/EMG recording post-saline or CNO (0.3 mg/kg) injections.

(K and L) Summarized changes of sleep duration (K) and latency (L) during the 6-h period post-injection.

(M) Average bout length in all vigilance states during 6 h of sleep recordings post-saline or CNO injection.

(N) Total bout counts in all vigilance states during 6 h of sleep recordings post-saline or CNO injection.

All data are presented as means ± SEM. Individual circles in the graphs indicate independent mice used per experiment. $*p < 0.05$ and $**p < 0.01$, paired *t* test. See also Figures S2 and S3.

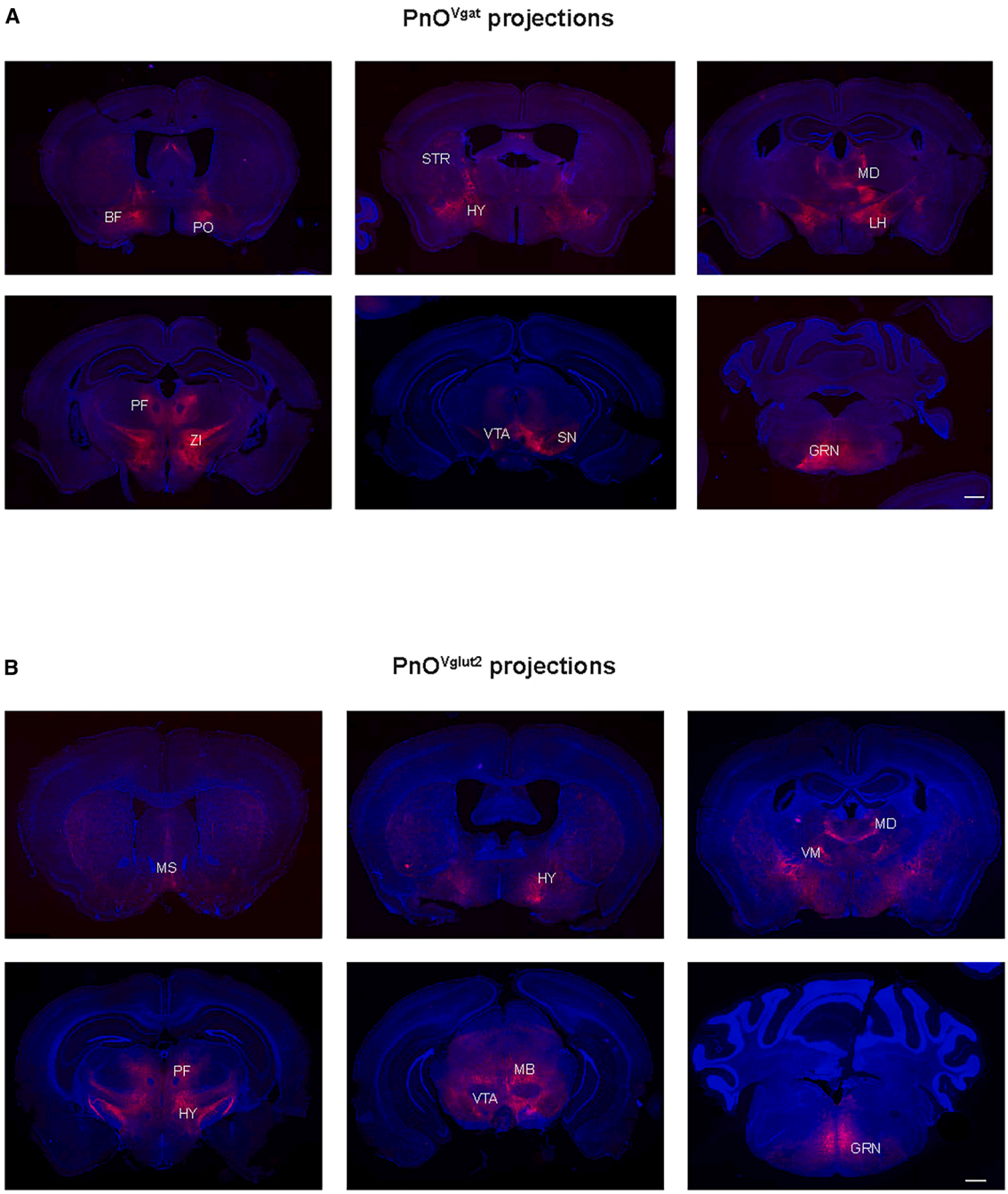

Figure 3. PnO GABAergic and glutamatergic neurons project to various sleep-wake regulating brain areas

(A) Representative images of projections from PnO$^{Vgat\text{-}mCherry}$ neurons.

(B) Representative images of projections from PnO$^{Vgat\text{-}mCherry}$ neurons.

Abbreviations are as follows: BF, basal forebrain; PO, preoptic area; STR, striatum; HY, hypothalamus; MD, mediodorsal nucleus of thalamus; MB, midbrain; LH, lateral hypothalamus; PF, parafascicular nucleus; ZI, zona inserta; VTA, ventral tegmental area; SN, substantia nigra; and GRN, gigantocellular reticular nucleus. Scale bars, 500 μm.

compartments and enriched with synaptic proteins.[35,36] By western blot analysis (Figure 6B), both SD and RS groups contained significantly more (around 2-fold) GluA1 AMPA receptor subunits in the PnO than the control PnO region from non-sleep-deprived animals, as well as enhanced protein levels (~25%) of the postsynaptic structural protein of excitatory synapses, PSD95, a protein that enhances insertion of AMPA receptors into synapses.[37,38] As an additional control, levels of GluA1 AMPA subunits in cerebellum samples from the same animals were not changed (Figure 6C). Elevated protein levels

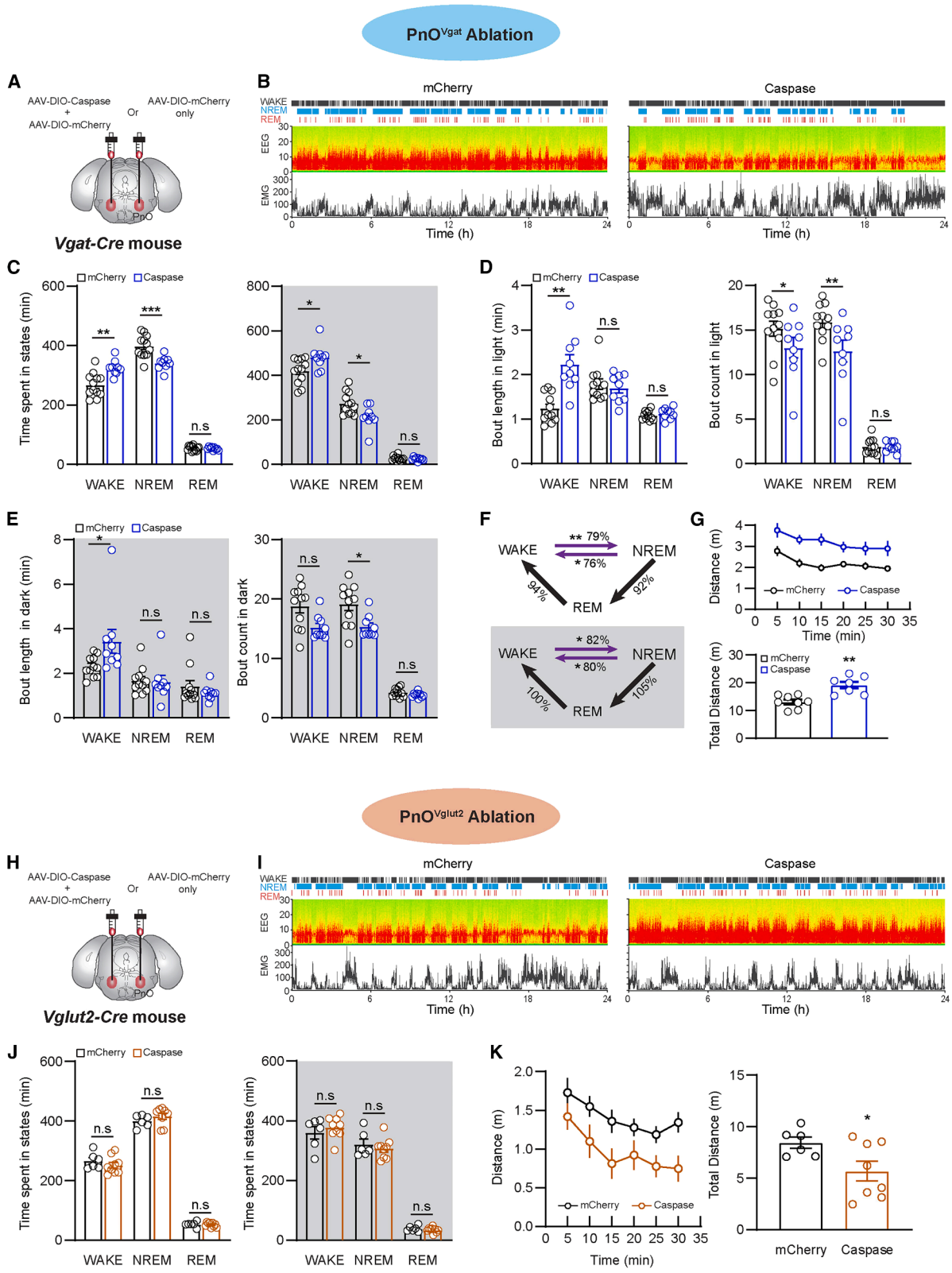

Figure 4. Genetic ablation of PnO^{Vgat} neurons suppresses sleep, and lesioning PnO^{Vglut2} neurons reduces locomotion

(A–G) Effects of selective ablation of PnO^{Vgat} neurons.

(A) Experimental setup.

(legend continued on next page)

(approximately 2-fold increase) of the activated (phosphorylated) catalytic subunits of PKA(T197)[39] and (approximately 4-fold increase) CaMKII(T286),[40] again starting in SD and being maintained through RS, were also detected (Figure 6B). Correspondingly, strongly increased levels of the phosphorylated form of GluA1 at S831 and S845, mediated by PKA and CaMKII, were also detected in PnO synaptoneurosomes during SD and in the subsequent RS. Phosphorylation at these serine sites on GluA1 could indicate enhanced synaptic transmission.[41,42] By contrast, protein levels in the PnO of GluA2 or GluA3 AMPA receptor subunits and the GluN1 NMDA-type glutamate receptor subunit were unchanged during SD and RS (Figure 6C). As a presynaptic marker, levels of synaptophysin protein, a component of synaptic vesicles, were also unchanged during SD and RS (Figure 6C).

Next, we assessed functional changes of AMPA receptors, and thus excitatory transmission, on individual PnO^{Vgat} neurons. To do this, *AAV-DIO-GFP* was bilaterally injected into the PnO of *Vgat-Cre* mice for visualizing PnO^{Vgat} neurons, and subsequently, mice were then either given 5 h SD and 1 h of RS or experienced the same total period of baseline sleep-wake activity. Acute brain slices of the PnO area were then prepared, and whole-cell voltage-clamp recordings were made from GFP-positive cells. For the PnO^{Vgat} neurons from mice that had 1 h RS, the AMPA/NMDA receptor ratio significantly increased by about 50% compared with the control neurons, thus showing enhanced incorporation of AMPA receptors onto the postsynaptic sites of the PnO^{Vgat} neurons (Figure 6D).

Collectively, these results reveal that during, or because of, extended wakefulness, levels of activated serine kinases (PKA and CaMKII), synaptic scaffolding proteins (PSD95), and GluA1 AMPA receptor subunits and associated serine phosphorylation increase. This all points to GluA1 AMPA receptor-mediated enhancement of glutamatergic excitatory transmission onto PnO^{Vgat} neurons as a potential mechanism that is already happening during SD and then contributes to enhancing the EEG delta power in RS and potentially contributes to the sustained but slow recovery of sleep.

DISCUSSION

Our study reveals that long-range projecting PnO^{Vgat} cells (the majority of which express the peptide somatostatin and the calcium-binding protein parvalbumin) are a component of the sleep homeostasis system, regulating both the transient delta power increase after SD and also contributing to the rate of sleep recovery in the subsequent 19 h post-SD. Within the PnO, we identified GABAergic PnO^{Vgat} neurons, but not the intermingled NREMS-inducing GABA/glycinergic PnO^{GlyT2} or WAKE-inducing glutamatergic PnO^{Vglut2} neurons, as uniquely able to switch their calcium activities (and thus likely action potential firing) in response to sleep pressure. In baseline conditions, PnO^{Vgat} neurons have the highest Ca^{2+} levels in WAKE and REMS. But during SD and in the subsequent first 2 h of RS, Ca^{2+} spiking increases significantly in these neurons. They then revert to lower Ca^{2+} levels by the third hour of RS. This raised Ca^{2+} during the first 2 h of NREM RS could be either associated with the cells' firing action potentials to drive the first stages of RS, such as the heightened EEG delta power, or alternatively, the Ca^{2+} could be functioning as a second messenger to ensure medium-term changes and that the subsequent RS is implemented by these cells. In parallel, starting during SD and persisting for the first 2 h of RS, levels of structural postsynaptic protein PSD95 increase, along with increased protein levels of activated PKA (pT197) and activated kinase CaMKII (pT286). The result is that GluA1-containing AMPA receptors with phosphorylated serines at positions 831 and 845, two modifications that facilitate enhanced synaptic transmission,[41,42] are functionally upregulated, as confirmed by an increased AMPA/NMDA glutamate receptor ratio found by whole-cell recording from PnO^{Vgat} cells. These changes, which do not happen in a non-sleep-regulating structure, the cerebellum, might allow PnO^{Vgat} neurons to initiate RS and implement sleep homeostatic control. Without PnO^{Vgat} neurons, there is no increase in delta EEG power straight after SD, and the rate of recovery of lost sleep, although not abolished, is significantly slowed, such that only around 50% of the lost sleep was recovered after 19 h.

The upstream glutamate terminals that drive the PnO^{Vgat} cells during RS could be from the local PnO^{Vglut2} neurons, although these did not change their Ca^{2+} activity during RS, or be long-range inputs from elsewhere in the brain. However, the activity and output of the upstream neurons may not need to change in response to SD, as upregulating postsynaptic AMPA receptors will be sufficient to produce more responses (i.e., the response to sleep pressure is only postsynaptic).

(B) Representative EEG/EMG recording across 24 h in control mCherry and PnO^{Vgat} caspase groups.
(C) Summary of total amount of time for both control (black) and caspase (blue) mice spent in WAKE, NREMS, and REMS states in the 12 h of light period or 12 h of dark period (with gray background).
(D) Left, average bout length during 12 h of light phase; right, average bout counts during 12 h of light phase.
(E) Left, average bout length during 12 h of dark phase; right, average bout counts during 12 h of dark phase.
(F) Reduced transitions between WAKE and NREMS states in the caspase mice compared to controls in both light and dark periods.
(G) 30 min open-field test on *Vglut2-Cre* mice. Top, travel distances in both mCherry control (black) and caspase (blue) groups plotted every 5 min. Bottom, average total travel distances during 30 min tests in both control and caspase groups.
(H–K) Effects of selective ablation of PnO^{Vglut2} neurons.
(H) Experimental setup.
(I) Representative EEG/EMG recording across 24 h in control mCherry and caspase groups.
(J) Summary of total amount of time for both control (black) and caspase (orange) mice spent in WAKE, NREMS, and REMS states in the 12 h of light period or 12 h of dark period (with gray background).
(K) Left, travel distances in both mCherry control (black) and caspase (orange) groups plotted every 5 min; Right, average total travel distances during 30 min tests in both control and caspase groups.
All data are presented as means ± SEM. Individual circles in the graphs indicate independent mice used per experiment. $^{*}p < 0.05$ and $^{**}p < 0.01$, *t* test.
See also Figure S4.

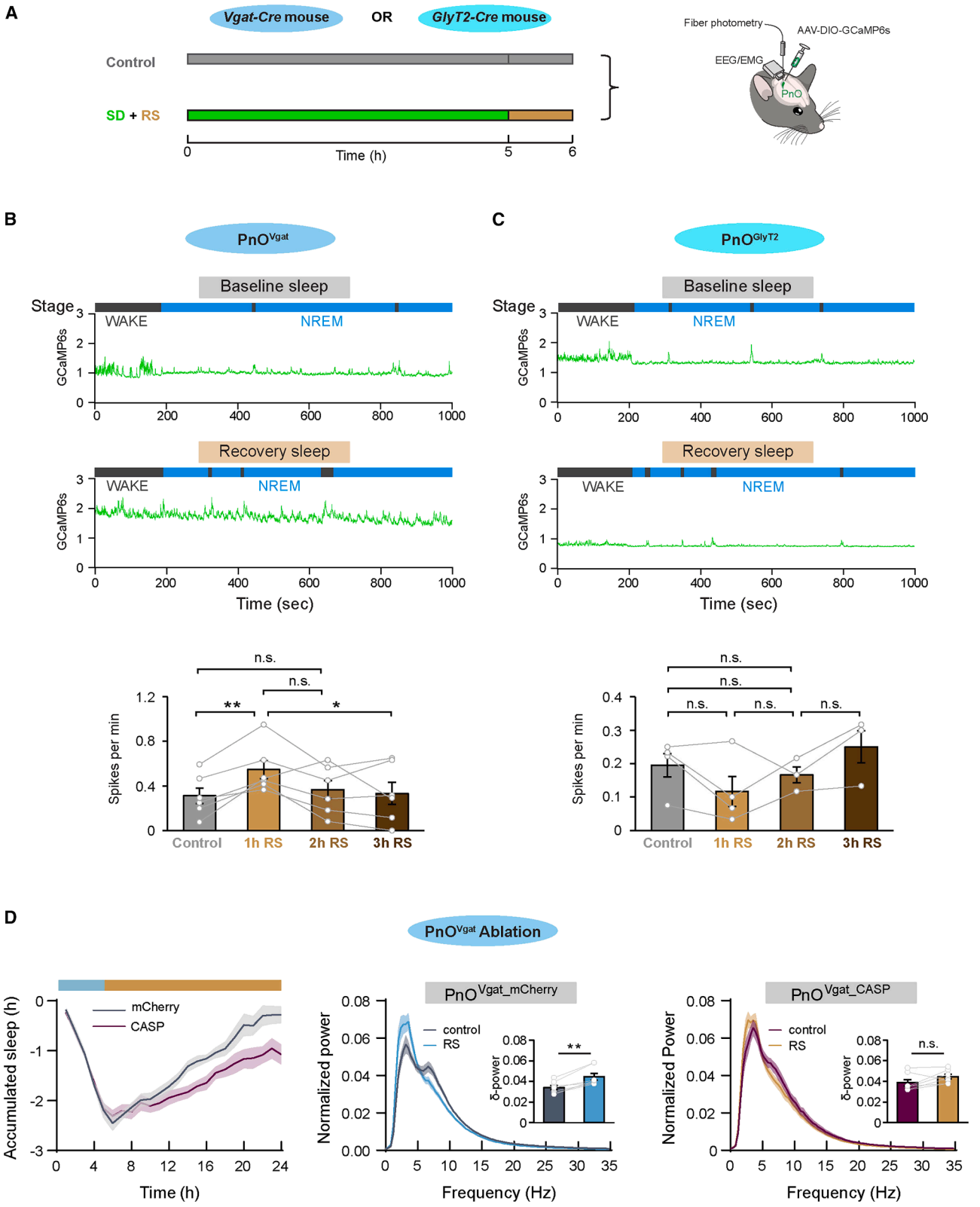

(legend on next page)

Our work builds on previous ideas as follows: although many synaptic proteins become phosphorylated following SD or time spent awake,[43–46] one simple change stands out. It is long established that as wakefulness progresses, GluA1 AMPA receptor amounts, and serine 831 and 845 phosphorylation of this subunit on the C terminus, increase, and that both GluA1 levels and serine phosphorylation decrease during sleep.[21] This is suggested to enable rebalancing of synaptic strengths and as a purpose of sleep (the SHY hypothesis).[19,20] More phosphorylated GluA1-containing AMPA receptors correspond to enhanced transmission at glutamate synapses between excitatory cells. However, for this particular PnO circuit, we are proposing that this SHY mechanism is adapted for catching up on sleep. As WAKE progresses, GluA1 phosphorylation and the AMPA/NMDA receptor ratio increase in PnO^{Vgat} cells, and then, in conjunction with (unknown) upstream glutamate neuronal input, this enhanced AMPA receptor expression is the basis for catching up on sleep. NREMS is initiated by the dedicated circuitry of the PnO^{Vgat} cells (but not the glycinergic cells).

Mechanism of plasticity (increased synaptic drive) onto PnO^{Vgat} neurons that could ensure enhanced recovery sleep

Many different changes in PnO^{Vgat} neurons, enhancing communication between excitatory neurons and PnO^{Vgat} neurons, could happen in parallel and reinforce each other during SD. An interesting feature is the increase in protein levels of PSD95, CaMKII, and PKA kinases, as well as GluA1 subunits (but not the other AMPA subunits or the NMDA GluN1 subunit). It is unclear how this protein level change happens, but if this occurs on dendrites of PnO^{Vgat} cells, then there could be local increases of mRNA translation of dendritic mRNA, as found in the hippocampus.[47] Post-synaptically, working as a structural protein in spines, CaMKII (pT286) is important for initiating structural changes that in themselves could increase plasticity independent of any kinase activity, as well as functioning as a kinase that initiates plasticity (both increases and decreases).[48] During SD, pulses of Ca^{2+} will increase the activity of CaMKII, resulting in autophosphorylation, and then the protein becomes Ca^{2+} independent.[48] Increasing the levels of the scaffold PSD95 protein will strongly promote insertion of AMPA receptors into the synapse, even without changing GluA1 levels.[37,38] PKA, anchored to AKAP scaffold proteins, once activated by cyclic AMP (Camp), can phosphorylate, together with CaMKII, AMPA GluA1 subunits. Both kinases work together to enhance AMPA receptor function. CaMKII-mediated serine 831 phosphorylation of the GluA1 AMPA subunit C-terminal segment increases single-channel conductance of the AMPA receptor[49]; PKA-mediated serine 845 phosphorylation on GluA1 increases both membrane insertion of receptors containing the subunit, and the single-channel conductance.[50–52] It has been claimed, based on whole-brain knockouts, that PKA is a "wake-promoting kinase"[44]; however, this is likely to depend on the type of cell in which PKA is expressed, as here we are positing that PKA is a "sleep-promoting kinase" in PnO^{Vgat} neurons.

Going forward, the relative contributions of these molecular pathways that allow PnO^{Vgat} cells to regulate sleep homeostasis could be dissected using approaches such as expressing phospho-mimetic mutations (S831D/S845D) in GluA1[53]; dominant-negative constructs that block AMPA receptor function[54]; dominant-active (CaMKIIα T286D) or kinase-dead CaMKIIα (K42R:T286D) variants, and CN19o, a CaMKII inhibitory peptide; and dominant-negative PSD95.[38]

Consistent with our findings, another study found that parvalbumin-positive cells in mice contribute to sleep homeostasis (increased delta power and sleep rebound) and that this requires CaMKII activation in those cells.[8] Although those authors inferred the cells to be neocortical, these parvalbumin neurons may also include the brainstem PnO^{Vgat} population we targeted by stereotaxic AAV injection (because in the other study, AAV delivery and transgenesis were via the optic nerve and so targeted parvalbumin cells throughout the brain).[8] Indeed, CaMKII has been described as a sleep-promoting kinase, as its gene knockout from the whole mouse reduces total NREMS by about an hour.[55]

It seems likely that for the PnO^{Vgat} neurons to fire more following SD, the end effect of the above processes, such as kinase activation and changes in scaffold proteins, must be to change channel or receptor function. AMPA-type glutamate receptors are the main basis for fast (millisecond scale) excitatory transmission in the brain. They are cation channels, mostly Ca^{2+}-impermeable, and made as heteromeric combinations of tetramers assembled from four possible AMPA receptor subunits (GluA1-4), with the composition (e.g., GluA1/GluA2) varying with cell type and brain region.[56,57] AMPA receptors without the GluA2 subunit, however, are Ca^{2+}-permeable,[58] although it is now thought that there is a continuum of AMPA receptors containing GluA2 subunits that can have Ca^{2+} permeability depending on the association of the receptor complexes with auxiliary proteins.[59] However, it is interesting to note that, although native Ca^{2+}-permeable AMPA receptors are typically GluA1/GluA4 heteromers,[60,61] GluA1 can function as a Ca^{2+}-permeable

Figure 5. GABAergic neurons in the PnO switch to NREMS-active mode during recovery sleep and are essential for normal sleep homeostatic responses

(A) Experimental setup. *Vgat-Cre* or *GlyT2-Cre* mice injected with *AAV-DIO-GCaMP6s* in the PnO were randomly assigned to control (undisturbed sleep) and recovery sleep (RS, 1 h sleep following 5 h of sleep deprivation) groups. Ca^{2+} transients of PnO^{Vgat} or PnO^{GlyT2} neurons were recorded using fiber photometry and compared at the same circadian time points.

(B) Top, representative fiber photometry recordings of PnO^{Vgat} neurons under baseline sleep and RS. Bottom, quantification of spike rates in controls, 1, 2, and 3 h of RS. Error bars represent SEMs. Individual circles in the graphs indicate independent mice used per experiment. $^{*}p < 0.05$ and $^{**}p < 0.01$.

(C) Top, representative fiber photometry recordings of PnO^{GlyT2} neurons under baseline sleep and recovery sleep. Bottom, quantification of spike rates in controls, 1, 2, and 3 h of RS.

(D) Homeostatic responses of mice with *AAV-DIO-mCherry* infected (control) or selective PnO^{Vgat} neurons ablated with *AAV-DIO-Capsase*. Left, slower recovery following 5 h of SD in the caspase group compared with controls. Middle and Right, normalized delta power during the first 2 h of RS in the control and PnO$^{Vgat\text{-}CASP}$ mice. Delta power accumulation is eliminated after selective ablation of PnO^{Vgat} neurons. Shaded bands represent the SEMs.

See also Figures S5 and S6.

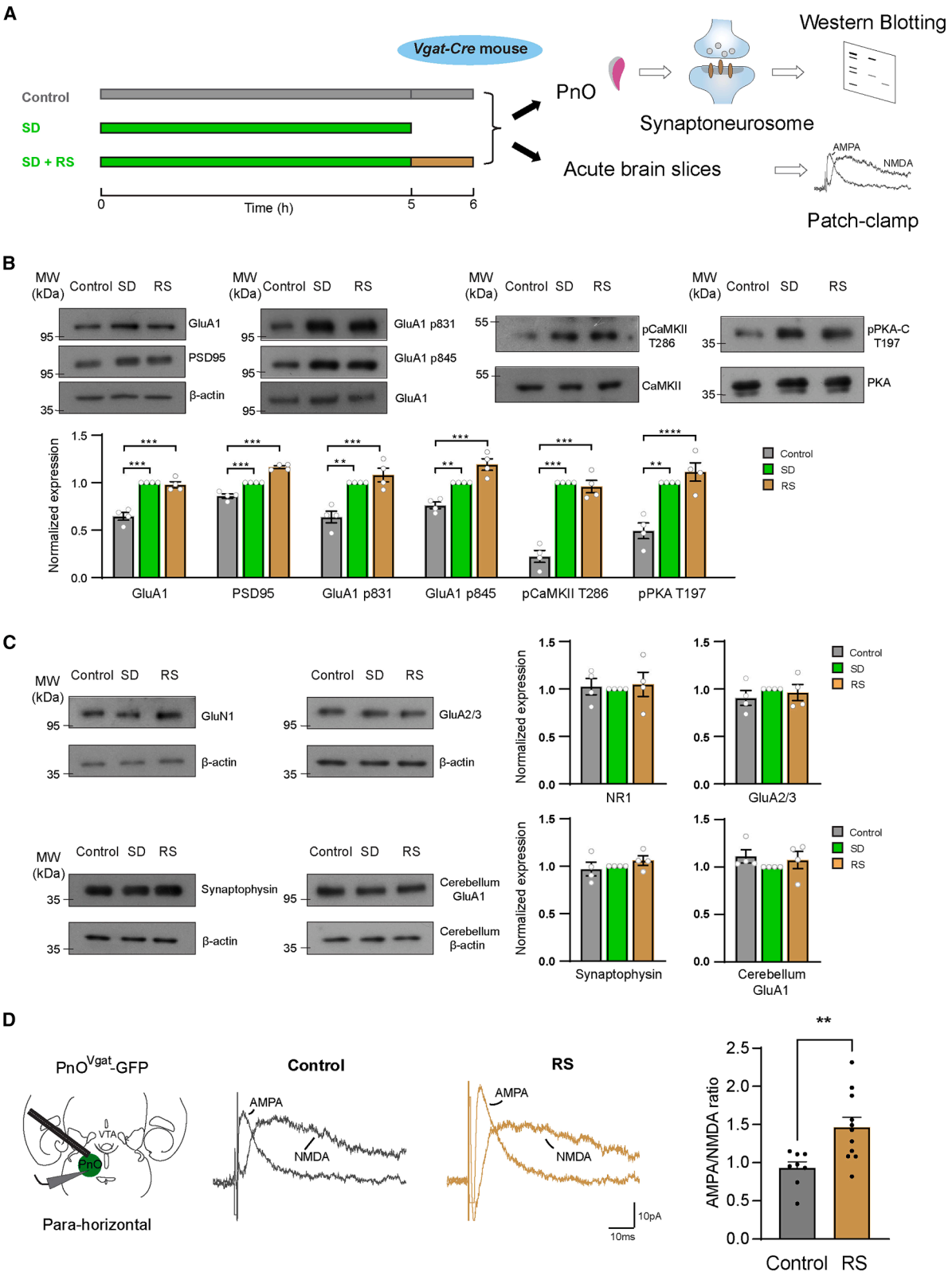

Figure 6. Enhanced synaptic strength in the PnO GABAergic neurons during recovery sleep following prolonged wakefulness

(A) Experimental setup. *Vgat-Cre* mice were randomly assigned to three groups: control, 5 h of sleep deprivation (SD), and recovery sleep (RS, 5 h of SD followed by 1 h of RS). Changes in synaptic strength were assessed using biochemical and electrophysiological methods. First, synaptoneurosomes were extracted from

(legend continued on next page)

homomeric receptor that contributes to plasticity,[62] and that increased amounts of GluA1 homomeric receptors in PnO^{Vgat} cells could explain the enhanced Ca^{2+} signal. The Ca^{2+} through these receptors could have further second messenger roles to ensure that PnO^{Vgat} cells stay active following SD.

Beyond the simple concept of synaptic plasticity, an intriguing alternative explanation for our findings is that activity in PnO^{Vgat} neurons during extended wakefulness alters the maintenance of excitatory synapse diversity, thereby changing PnO^{Vgat} output and sleep drive. We measured plasticity at the cell population level (western blot, electrophysiology), but single-synapse analyses reveal a striking synapse diversity across the mouse brain,[63] and this diversity is modified by SD.[18] Different synapse types and subtypes show distinct, activity-dependent protein turnover rates.[18,63,64] Thus, it could be that in PnO neurons, proteostatic mechanisms regulating excitatory synaptic diversity could track sleep pressure and adjust NREMS accordingly. A next step would be to characterize the PnO^{Vgat} "synaptome," its protein composition and turnover, at high spatial resolution in identified PnO neurons during extended WAKE.

An unexpected finding of our study is that WAKE/REMS-active PnO^{Vgat} (and PnO^{GlyT2}) neurons (inferred by Ca^{2+} photometry) promoted NREMS when chemo-activated. Similar results, with mismatches between neurons having WAKE/REMS Ca^{2+} signals, but when they are chemo- or opto-activated, induce NREMS, have been reported by us and others before. Examples include GABAergic neurons in the VTA, parvalbumin-expressing neurons in the ventral medulla, and glutamatergic neurons in the lateral habenula (LHb).[65–67] Given that the GABA neurons in the VTA also contribute to catching up on lost sleep after SD,[12] it may be that these neurons can also switch their activity from WAKE/REMS to NREMS. On the other hand, the PnO^{GlyT2} neurons do not switch their Ca^{2+} levels during SD.

What triggers the SHY-like mechanism in PnO^{Vgat} neurons during SD? Most models of sleep homeostasis in mammals focus on molecular mechanisms that affect the increase in EEG delta power post-SD, but do not usually examine the actual catching up on lost sleep. There are many substances and biochemical reactions that change with time spent awake, thus potentially providing a mechanism to track wakefulness and sleep pressure, and which could be influencing PnO^{Vgat} neurons. These factors include accumulating extracellular adenosine,[68,69] increasing intracellular chloride concentrations,[70] and increasing non-mitochondrial cytosolic hydrogen peroxide.[71] In fruit flies, changes in mitochondrial oxidation state and accumulating lipid peroxidation contribute to the origin of sleep pressure.[4,72] All these substances, or biochemical changes, are suggested to result in a threshold being passed because of prolonged wakefulness and the activation of sleep-promoting neurons. Mutations in several of the biochemical pathways, such as the LKB1 kinase-Sik3-HDAC pathway, that regulate the overall amount of sleep in any given 24-h period, although influencing the transient delta power increase after SD, do not result in the mice catching up on lost sleep.[46] On the other hand, calcineurin phosphatase knockouts throughout the mouse brain reduce the ability to catch up on lost sleep.[73]

Arousal-promoting neurons in the PnO

We discovered an intermingled population of glutamate neurons in the PnO that affected locomotion. Their lesioning did not affect baseline sleep-wake states, but mice became hypomobile after specific lesioning of these cells. The effects of extended wakefulness upon chemo-activation of these neurons lasted for 9 h, greater than those of glutamatergic populations in wake-promoting areas such as the preoptic area (POA), LH, and medial septum (MS),[74–76] but comparable in duration to chemo-activation of wake-promoting glutamatergic/nitrergic cells in the VTA.[65] When activated, the PnO glutamatergic neurons likely engage multiple wake-related brain regions (see Figure 3) to achieve arousal, for example, the midline thalamic nuclei (Figure 3). Although lesions or selective inhibitions of various wake-promoting neuronal populations have little effect on baseline sleep-wake durations,[77–80] these kinds of neurons often mediate arousal under specific conditions, such as exposure to a novel environment, waking from a loud sound, or other stressors.[81–83] Thus, PnO^{Vglut2} neurons could have similar roles. Also, an anesthetic-sensitive region in the rat brainstem, termed the mesopontine tegmental anesthesia area, where microinjections of various anesthetic agents rapidly and reversibly induce general anesthesia,[84,85] overlaps with the PnO area.[86,87] How PnO neurons respond to anesthetics or facilitate emergence and recovery from general anesthesia requires future investigation.

Conclusions

Our results add weight to the idea that sleep drive is encoded by synaptic plasticity (see background material in the introduction) and that sleep homeostasis is regulated by distributed circuits. Intriguingly, the molecular changes (e.g., serine phosphorylated AMPA GluA1 receptor subunits, increased CaMKII levels) in PnO^{Vgat} neurons that seem likely to drive increased sleep are similar to those that form the foundations of SHY,[21] whereby those markers increase during WAKE, reflecting more potentiation between excitatory cells in the neocortex and hippocampus, and then become reset during NREMS.[16,22,23] We propose that a SHY-like mechanism between excitatory and inhibitory neurons in the PnO can also be used to implement sleep homeostasis.

the PnO, and expression of key synaptic proteins was examined using western blotting. Second, acute brain slices containing the PnO area were prepared from *Vgat-Cre mice* injected with *AAV-DIO-GFP* to label GABAergic neurons. AMPA/NMDA receptor ratios were recorded and compared in three experimental groups.

(B) Top, representative images of western blotting of synaptic proteins including GluA1 AMPA receptor subunit, PSD95, GluA1 p831 and p845, pCaMKII T286, and pPKA-C T197. Bottom, normalized expression of examined synaptic proteins.

(C) No changes were detected in GluN1 NMDA receptor, GluA2/3 AMPA receptor, synaptophysin, or cerebellar GluA1 AMPA receptor protein levels.

(D) Left, experimental setup for the electrophysiology. Middle, example traces of evoked AMPA receptor- and NMDA receptor-mediated currents recorded using whole-cell patch clamp. Right, AMPA/NMDA ratio in control and RS groups. Dots represent individual animals.

All data are presented as means ± SEM. Individual circles in the graphs indicate independent mice used per experiment. *$p < 0.05$, **$p < 0.01$, ***$p < 0.001$, and****$p < 0.0001$; *t* test.

RESOURCE AVAILABILITY

Lead contact

Further information and requests for resources and reagents should be directed to and will be fulfilled by the lead contact, Nicholas P. Franks (n.franks@imperial.ac.uk).

Materials availability

This study did not generate new, unique reagents.

Data and code availability

- All datasets generated in this study are available on Mendeley Data (10.17632/hzkpzsd8f9.1).
- This paper does not report original code.
- Any additional information required to reanalyze the data reported in this paper is available from the lead contact upon request.

ACKNOWLEDGMENTS

We thank The Turku Screening Unit of the Drug Discovery and Chemical Biology platform of Biocentre Finland for the support of biochemical analysis, D. Gaboriau (Imperial College) for the technical support with the microscopes, and V. Navetat and E. Beckwith for helping with some of the illustrations. This work was supported by grants from: the Wellcome Trust (220759/Z/20/Z to N.P.F. and W.W.), the UK Dementia Research Institute (UK DRI-5004 to N.P.F. and W.W.), the Medical Research Council (APP9329 to N.P.F., S.W., and W.W.), the Rubicon Research Program of the Netherlands Organization for Scientific Research (NWO) (019.161LW.010 to W.B.), the People Program (Marie Curie Actions) of the European Union's Eight Framework Program H2020 under REA grant agreement 753548 (to W.B.), the Research Council of Finland (grant nos. 348983 to M.J.C. and 346939 to L.-L.L.) and the Magnus Ehrnrooth Foundation, Finland (to L.-L.L.). The Facility for Imaging by Light Microscopy (FILM) at Imperial College London was in part supported by funding from the Wellcome Trust (grant 104931/Z/14/Z) and BBSRC (grant BB/L015129/1).

AUTHOR CONTRIBUTIONS

The project was supervised by N.P.F. and W.W. Experiments were designed by W.B., E.C.H., N.P.F., and W.W. Experiments were performed by W.B., E.C.H., M.N., L.-L.L., K.T., L.L., R.Y., J.O., B.A.S., and S.W., and analyzed by W.B., E.C.H., L.-L.L., and K.T. Resources were provided by A.L.V., M.J.C., and H.U.Z. The manuscript was written, reviewed, and edited by W.B., E.C.H., N.P.F., and W.W. Funding was granted to N.P.F., W.W., W.B., L.-L.L., and M.J.C.

DECLARATION OF INTERESTS

The authors declare they have no competing interests.

STAR★METHODS

Detailed methods are provided in the online version of this paper and include the following:

- KEY RESOURCES TABLE
- EXPERIMENTAL MODEL AND STUDY PARTICIPANT DETAILS
  - Mice
- METHOD DETAILS
  - Viral constructs and preparation
  - Stereotaxic surgery
  - EEG and EMG recording and scoring of sleep-wake states
  - Sleep deprivation
  - Immunohistochemistry
  - Fiber photometry
  - Synaptoneurosomal preparation
  - Immunoblotting
  - Acute slice electrophysiology recordings and single-cell RT-qPCR
- QUANTIFICATION AND STATISTICAL ANALYSIS

SUPPLEMENTAL INFORMATION

Supplemental information can be found online at https://doi.org/10.1016/j.cub.2026.04.059.

Received: October 17, 2025
Revised: March 24, 2026
Accepted: April 24, 2026
Published: May 19, 2026

REFERENCES

1. Franks, N.P., and Wisden, W. (2021). The inescapable drive to sleep: Overlapping mechanisms of sleep and sedation. Science *374*, 556–559. https://doi.org/10.1126/science.abi8372.
2. Franken, P., and Dijk, D.J. (2024). Sleep and circadian rhythmicity as entangled processes serving homeostasis. Nat. Rev. Neurosci. *25*, 43–59. https://doi.org/10.1038/s41583-023-00764-z.
3. Borbely, A.A. (1982). A two process model of sleep regulation. Hum. Neurobiol. *1*, 195–204.
4. Sarnataro, R., Velasco, C.D., Monaco, N., Kempf, A., and Miesenböck, G. (2025). Mitochondrial origins of the pressure to sleep. Nature *645*, 722–728. https://doi.org/10.1038/s41586-025-09261-y.
5. Vyazovskiy, V.V., Olcese, U., Hanlon, E.C., Nir, Y., Cirelli, C., and Tononi, G. (2011). Local sleep in awake rats. Nature *472*, 443–447. https://doi.org/10.1038/nature10009.
6. Tossell, K., Yu, X., Giannos, P., Anuncibay Soto, B., Nollet, M., Yustos, R., Miracca, G., Vicente, M., Miao, A., Hsieh, B., et al. (2023). Somatostatin neurons in prefrontal cortex initiate sleep-preparatory behavior and sleep via the preoptic and lateral hypothalamus. Nat. Neurosci. *26*, 1805–1819. https://doi.org/10.1038/s41593-023-01430-4.
7. Krone, L.B., Yamagata, T., Blanco-Duque, C., Guillaumin, M.C.C., Kahn, M.C., van der Vinne, V., McKillop, L.E., Tam, S.K.E., Peirson, S.N., Akerman, C.J., et al. (2021). A role for the cortex in sleep-wake regulation. Nat. Neurosci. *24*, 1210–1215. https://doi.org/10.1038/s41593-021-00894-6.
8. Kon, K., Ode, K.L., Mano, T., Fujishima, H., Takahashi, R.R., Tone, D., Shimizu, C., Shiono, S., Yada, S., Matsuzawa, K., et al. (2024). Cortical parvalbumin neurons are responsible for homeostatic sleep rebound through CaMKII activation. Nat. Commun. *15*, 6054. https://doi.org/10.1038/s41467-024-50168-5.
9. Zhang, Z., Ferretti, V., Güntan, İ., Moro, A., Steinberg, E.A., Ye, Z., Zecharia, A.Y., Yu, X., Vyssotski, A.L., Brickley, S.G., et al. (2015). Neuronal ensembles sufficient for recovery sleep and the sedative actions of α2 adrenergic agonists. Nat. Neurosci. *18*, 553–561. https://doi.org/10.1038/nn.3957.
10. Ma, Y., Miracca, G., Yu, X., Harding, E.C., Miao, A., Yustos, R., Vyssotski, A.L., Franks, N.P., and Wisden, W. (2019). Galanin Neurons Unite Sleep Homeostasis and alpha2-Adrenergic Sedation. Curr. Biol. *29*, 3315–3322.e3. https://doi.org/10.1016/j.cub.2019.07.087.
11. Reichert, S., Pavón Arocas, O., and Rihel, J. (2019). The Neuropeptide Galanin Is Required for Homeostatic Rebound Sleep following Increased Neuronal Activity. Neuron *104*, 370–384.e5. https://doi.org/10.1016/j.neuron.2019.08.010.
12. Yu, X., Ba, W., Zhao, G., Ma, Y., Harding, E.C., Yin, L., Wang, D., Li, H., Zhang, P., Shi, Y., et al. (2021). Dysfunction of ventral tegmental area GABA neurons causes mania-like behavior. Mol. Psychiatry *26*, 5213–5228. https://doi.org/10.1038/s41380-020-0810-9.
13. Oikonomou, G., Altermatt, M., Zhang, R.W., Coughlin, G.M., Montz, C., Gradinaru, V., and Prober, D.A. (2019). The Serotonergic Raphe Promote Sleep in Zebrafish and Mice. Neuron *103*, 686–701.e8. https://doi.org/10.1016/j.neuron.2019.05.038.
14. Lee, S.S., Liu, Q., Cheng, A.H.R., Kim, D.W., Boudreau, D.M., Mehta, A., Keles, M.F., Fejfer, R., Palmer, I., Park, K.H., et al. (2025). Sleep

need-dependent plasticity of a thalamic circuit promotes homeostatic recovery sleep. Science *388*, eadm8203. https://doi.org/10.1126/science.adm8203.

15. Puentes-Mestril, C., and Aton, S.J. (2017). Linking Network Activity to Synaptic Plasticity during Sleep: Hypotheses and Recent Data. Front. Neural Circuits *11*, 61. https://doi.org/10.3389/fncir.2017.00061.
16. de Vivo, L., Bellesi, M., Marshall, W., Bushong, E.A., Ellisman, M.H., Tononi, G., and Cirelli, C. (2017). Ultrastructural evidence for synaptic scaling across the wake/sleep cycle. Science *355*, 507–510. https://doi.org/10.1126/science.aah5982.
17. Suppermpool, A., Lyons, D.G., Broom, E., and Rihel, J. (2024). Sleep pressure modulates single-neuron synapse number in zebrafish. Nature *629*, 639–645. https://doi.org/10.1038/s41586-024-07367-3.
18. Koukaroudi, D., Qiu, Z., Fransén, E., Gokhale, R., Bulovaite, E., Komiyama, N.H., Seibt, J., and Grant, S.G.N. (2024). Sleep maintains excitatory synapse diversity in the cortex and hippocampus. Curr. Biol. *34*, 3836–3843.e5. https://doi.org/10.1016/j.cub.2024.07.032.
19. Tononi, G., and Cirelli, C. (2003). Sleep and synaptic homeostasis: a hypothesis. Brain Res. Bull. *62*, 143–150. https://doi.org/10.1016/j.brainresbull.2003.09.004.
20. Tononi, G., and Cirelli, C. (2014). Sleep and the price of plasticity: from synaptic and cellular homeostasis to memory consolidation and integration. Neuron *81*, 12–34. https://doi.org/10.1016/j.neuron.2013.12.025.
21. Vyazovskiy, V.V., Cirelli, C., Pfister-Genskow, M., Faraguna, U., and Tononi, G. (2008). Molecular and electrophysiological evidence for net synaptic potentiation in wake and depression in sleep. Nat. Neurosci. *11*, 200–208. https://doi.org/10.1038/nn2035.
22. Squarcio, F., Tononi, G., and Cirelli, C. (2024). Effects of non-rapid eye movement sleep on the cortical synaptic expression of GluA1-containing AMPA receptors. Eur. J. Neurosci. *60*, 3961–3972. https://doi.org/10.1111/ejn.16460.
23. Diering, G.H., Nirujogi, R.S., Roth, R.H., Worley, P.F., Pandey, A., and Huganir, R.L. (2017). Homer1a drives homeostatic scaling-down of excitatory synapses during sleep. Science *355*, 511–515. https://doi.org/10.1126/science.aai8355.
24. Liu, S., Liu, Q., Tabuchi, M., and Wu, M.N. (2016). Sleep drive is encoded by neural plastic changes in a dedicated circuit. Cell *165*, 1347–1360. https://doi.org/10.1016/j.cell.2016.04.013.
25. Miracca, G., Anuncibay-Soto, B., Tossell, K., Yustos, R., Vyssotski, A.L., Franks, N.P., and Wisden, W. (2022). NMDA Receptors in the Lateral Preoptic Hypothalamus Are Essential for Sustaining NREM and REM Sleep. J. Neurosci. *42*, 5389–5409. https://doi.org/10.1523/JNEUROSCI.0350-21.2022.
26. Sawada, T., Iino, Y., Yoshida, K., Okazaki, H., Nomura, S., Shimizu, C., Arima, T., Juichi, M., Zhou, S., Kurabayashi, N., et al. (2024). Prefrontal synaptic regulation of homeostatic sleep pressure revealed through synaptic chemogenetics. Science *385*, 1459–1465. https://doi.org/10.1126/science.adl3043.
27. Xi, M.C., Morales, F.R., and Chase, M.H. (1999). Evidence that wakefulness and REM sleep are controlled by a GABAergic pontine mechanism. J. Neurophysiol. *82*, 2015–2019. https://doi.org/10.1152/jn.1999.82.4.2015.
28. Sanford, L.D., Tang, X., Xiao, J., Ross, R.J., and Morrison, A.R. (2003). GABAergic regulation of REM sleep in reticularis pontis oralis and caudalis in rats. J. Neurophysiol. *90*, 938–945. https://doi.org/10.1152/jn.00993.2002.
29. Reinoso-Suárez, F., de Andrés, I., Rodrigo-Angulo, M.L., and Rodríguez-Veiga, E. (1994). Location and Anatomical Connections of a Paradoxical Sleep Induction Site in the Cat Ventral Pontine Tegmentum. Eur. J. Neurosci. *6*, 1829–1836. https://doi.org/10.1111/j.1460-9568.1994.tb00575.x.
30. Camacho-Arroyo, I., Alvarado, R., Manjarrez, J., and Tapia, R. (1991). Microinjections of muscimol and bicuculline into the pontine reticular formation modify the sleep-waking cycle in the rat. Neurosci. Lett. *129*, 95–97. https://doi.org/10.1016/0304-3940(91)90728-C.
31. Horner, R.L., and Kubin, L. (1999). Pontine carbachol elicits multiple rapid eye movement sleep-like neural events in urethane-anaesthetized rats. Neuroscience *93*, 215–226. https://doi.org/10.1016/S0306-4522(99)00126-8.
32. Nuñez, A., de Andrés, I., and García-Austt, E. (1991). Relationships of nucleus reticularis pontis oralis neuronal discharge with sensory and carbachol evoked hippocampal theta rhythm. Exp. Brain Res. *87*, 303–308. https://doi.org/10.1007/BF00231847.
33. Giber, K., Diana, M.A., M Plattner, V., Dugué, G.P., Bokor, H., Rousseau, C.V., Maglóczky, Z., Havas, L., Hangya, B., Wildner, H., et al. (2015). A subcortical inhibitory signal for behavioral arrest in the thalamus. Nat. Neurosci. *18*, 562–568. https://doi.org/10.1038/nn.3951.
34. Huganir, R.L., and Nicoll, R.A. (2013). AMPARs and synaptic plasticity: The last 25 years. Neuron *80*, 704–717. https://doi.org/10.1016/j.neuron.2013.10.025.
35. Villasana, L.E., Klann, E., and Tejada-Simon, M.V. (2006). Rapid isolation of synaptoneurosomes and postsynaptic densities from adult mouse hippocampus. J. Neurosci. Methods *158*, 30–36. https://doi.org/10.1016/j.jneumeth.2006.05.008.
36. Hollingsworth, E.B., McNeal, E.T., Burton, J.L., Williams, R.J., Daly, J.W., and Creveling, C.R. (1985). Biochemical characterization of a filtered synaptoneurosome preparation from guinea pig cerebral cortex: Cyclic adenosine 3′:5′-monophosphate-generating systems, receptors, and enzymes. J. Neurosci. *5*, 2240–2253. https://doi.org/10.1523/JNEUROSCI.05-08-02240.1985.
37. Schnell, E., Sizemore, M., Karimzadegan, S., Chen, L., Bredt, D.S., and Nicoll, R.A. (2002). Direct interactions between PSD-95 and stargazin control synaptic AMPA receptor number. Proc. Natl. Acad. Sci. USA *99*, 13902–13907. https://doi.org/10.1073/pnas.172511199.
38. Ehrlich, I., and Malinow, R. (2004). Postsynaptic density 95 controls AMPA receptor incorporation during long-term potentiation and experience-driven synaptic plasticity. J. Neurosci. *24*, 916–927. https://doi.org/10.1523/JNEUROSCI.4733-03.2004.
39. Humphries, K.M., Deal, M.S., and Taylor, S.S. (2005). Enhanced dephosphorylation of cAMP-dependent protein kinase by oxidation and thiol modification. J. Biol. Chem. *280*, 2750–2758. https://doi.org/10.1074/jbc.M410242200.
40. Giese, K.P., Fedorov, N.B., Filipkowski, R.K., and Silva, A.J. (1998). Autophosphorylation at Thr286 of the alpha calcium-calmodulin kinase II in LTP and learning. Science *279*, 870–873. https://doi.org/10.1126/science.279.5352.870.
41. Lee, H.K., Barbarosie, M., Kameyama, K., Bear, M.F., and Huganir, R.L. (2000). Regulation of distinct AMPA receptor phosphorylation sites during bidirectional synaptic plasticity. Nature *405*, 955–959. https://doi.org/10.1038/35016089.
42. Diering, G.H., and Huganir, R.L. (2018). The AMPA Receptor Code of Synaptic Plasticity. Neuron *100*, 314–329. https://doi.org/10.1016/j.neuron.2018.10.018.
43. Wang, Z., Ma, J., Miyoshi, C., Li, Y., Sato, M., Ogawa, Y., Lou, T., Ma, C., Gao, X., Lee, C., et al. (2018). Quantitative phosphoproteomic analysis of the molecular substrates of sleep need. Nature *558*, 435–439. https://doi.org/10.1038/s41586-018-0218-8.
44. Wang, Y., Cao, S., Tone, D., Fujishima, H., Yamada, R.G., Ohno, R.I., Shi, S., Matsuzawa, K., Yada, S., Kaneko, M., et al. (2024). Postsynaptic competition between calcineurin and PKA regulates mammalian sleep-wake cycles. Nature *636*, 412–421. https://doi.org/10.1038/s41586-024-08132-2.
45. Kim, S.J., Hotta-Hirashima, N., Asano, F., Kitazono, T., Iwasaki, K., Nakata, S., Komiya, H., Asama, N., Matsuoka, T., Fujiyama, T., et al. (2022). Kinase signalling in excitatory neurons regulates sleep quantity and depth. Nature *612*, 512–518. https://doi.org/10.1038/s41586-022-05450-1.

46. Zhou, R., Wang, G., Li, Q., Meng, F., Liu, C., Gan, R., Ju, D., Liao, M., Xu, J., Sang, D., et al. (2022). A signalling pathway for transcriptional regulation of sleep amount in mice. Nature *612*, 519–527. https://doi.org/10.1038/s41586-022-05510-6.

47. Giandomenico, S.L., Alvarez-Castelao, B., and Schuman, E.M. (2022). Proteostatic regulation in neuronal compartments. Trends Neurosci. *45*, 41–52. https://doi.org/10.1016/j.tins.2021.08.002.

48. Bayer, K.U., and Giese, K.P. (2025). A revised view of the role of CaMKII in learning and memory. Nat. Neurosci. *28*, 24–34. https://doi.org/10.1038/s41593-024-01809-x.

49. Kristensen, A.S., Jenkins, M.A., Banke, T.G., Schousboe, A., Makino, Y., Johnson, R.C., Huganir, R., and Traynelis, S.F. (2011). Mechanism of Ca2+/calmodulin-dependent kinase II regulation of AMPA receptor gating. Nat. Neurosci. *14*, 727–735. https://doi.org/10.1038/nn.2804.

50. Banke, T.G., Bowie, D., Lee, H.K., Huganir, R.L., Schousboe, A., and Traynelis, S.F. (2000). Control of GluR1 AMPA receptor function by cAMP-dependent protein kinase. J. Neurosci. *20*, 89–102. https://doi.org/10.1523/JNEUROSCI.20-01-00089.2000.

51. Diering, G.H., Gustina, A.S., and Huganir, R.L. (2014). PKA-GluA1 coupling via AKAP5 controls AMPA receptor phosphorylation and cell-surface targeting during bidirectional homeostatic plasticity. Neuron *84*, 790–805. https://doi.org/10.1016/j.neuron.2014.09.024.

52. Esteban, J.A., Shi, S.H., Wilson, C., Nuriya, M., Huganir, R.L., and Malinow, R. (2003). PKA phosphorylation of AMPA receptor subunits controls synaptic trafficking underlying plasticity. Nat. Neurosci. *6*, 136–143. https://doi.org/10.1038/nn997.

53. Makino, Y., Johnson, R.C., Yu, Y., Takamiya, K., and Huganir, R.L. (2011). Enhanced synaptic plasticity in mice with phosphomimetic mutation of the GluA1 AMPA receptor. Proc. Natl. Acad. Sci. USA *108*, 8450–8455. https://doi.org/10.1073/pnas.1105261108.

54. Stephenson-Jones, M., Yu, K., Ahrens, S., Tucciarone, J.M., van Huijstee, A.N., Mejia, L.A., Penzo, M.A., Tai, L.H., Wilbrecht, L., and Li, B. (2016). A basal ganglia circuit for evaluating action outcomes. Nature *539*, 289–293. https://doi.org/10.1038/nature19845.

55. Tatsuki, F., Sunagawa, G.A., Shi, S., Susaki, E.A., Yukinaga, H., Perrin, D., Sumiyama, K., Ukai-Tadenuma, M., Fujishima, H., Ohno, R., et al. (2016). Involvement of Ca(2+)-Dependent Hyperpolarization in Sleep Duration in Mammals. Neuron *90*, 70–85. https://doi.org/10.1016/j.neuron.2016.02.032.

56. Keinänen, K., Wisden, W., Sommer, B., Werner, P., Herb, A., Verdoorn, T.A., Sakmann, B., and Seeburg, P.H. (1990). A Family of Ampa-Selective Glutamate Receptors. Science *249*, 556–560. https://doi.org/10.1126/science.2166337.

57. Hansen, K.B., Wollmuth, L.P., Bowie, D., Furukawa, H., Menniti, F.S., Sobolevsky, A.I., Swanson, G.T., Swanger, S.A., Greger, I.H., Nakagawa, T., et al. (2021). Structure, Function, and Pharmacology of Glutamate Receptor Ion Channels. Pharmacol. Rev. *73*, 1469–1658. https://doi.org/10.1124/pharmrev.120.000131.

58. Hollmann, M., Hartley, M., and Heinemann, S. (1991). Ca2+ permeability of KA-AMPA–gated glutamate receptor channels depends on subunit composition. Science *252*, 851–853. https://doi.org/10.1126/science.1709304.

59. Miguez-Cabello, F., Wang, X.T., Yan, Y., Brake, N., Alexander, R.P.D., Perozzo, A.M., Khadra, A., and Bowie, D. (2025). GluA2-containing AMPA receptors form a continuum of Ca(2+)-permeable channels. Nature *641*, 537–544. https://doi.org/10.1038/s41586-025-08736-2.

60. Burnashev, N., Khodorova, A., Jonas, P., Helm, P.J., Wisden, W., Monyer, H., Seeburg, P.H., and Sakmann, B. (1992). Calcium-Permeable Ampa-Kainate Receptors in Fusiform Cerebellar Glial-Cells. Science *256*, 1566–1570. https://doi.org/10.1126/science.1317970.

61. Geiger, J.R.P., Melcher, T., Koh, D.S., Sakmann, B., Seeburg, P.H., Jonas, P., and Monyer, H. (1995). Relative abundance of subunit mRNAs determines gating and Ca2+ permeability of AMPA receptors in principal neurons and interneurons in rat CNS. Neuron *15*, 193–204. https://doi.org/10.1016/0896-6273(95)90076-4.

62. Ge, Y., and Wang, Y.T. (2021). GluA1-homomeric AMPA receptor in synaptic plasticity and neurological diseases. Neuropharmacology *197*, 108708. https://doi.org/10.1016/j.neuropharm.2021.108708.

63. Zhu, F., Cizeron, M., Qiu, Z., Benavides-Piccione, R., Kopanitsa, M.V., Skene, N.G., Koniaris, B., DeFelipe, J., Fransén, E., Komiyama, N.H., et al. (2018). Architecture of the Mouse Brain Synaptome. Neuron *99*, 781–799.e10. https://doi.org/10.1016/j.neuron.2018.07.007.

64. Bulovaite, E., Qiu, Z., Kratschke, M., Zgraj, A., Fricker, D.G., Tuck, E.J., Gokhale, R., Koniaris, B., Jami, S.A., Merino-Serrais, P., et al. (2022). A brain atlas of synapse protein lifetime across the mouse lifespan. Neuron *110*, 4057–4073.e8. https://doi.org/10.1016/j.neuron.2022.09.009.

65. Yu, X., Li, W., Ma, Y., Tossell, K., Harris, J.J., Harding, E.C., Ba, W., Miracca, G., Wang, D., Li, L., et al. (2019). GABA and glutamate neurons in the VTA regulate sleep and wakefulness. Nat. Neurosci. *22*, 106–119. https://doi.org/10.1038/s41593-018-0288-9.

66. Ba, W., Nollet, M., Yin, C., Yu, X., Wong, S., Miao, A., Beckwith, E.J., Harding, E.C., Ma, Y., Yustos, R., et al. (2024). A REM-active basal ganglia circuit that regulates anxiety. Curr. Biol. *34*, 3301–3314.e4. https://doi.org/10.1016/j.cub.2024.06.010.

67. Cleary, C.M., Souza, G.M.P.R., Abbott, S.B.G., and Mulkey, D.K. (2025). Parvalbumin-expressing neurons in the ventral medulla are active during wakefulness and promote NREM sleep. Sleep *48*, zsaf118. https://doi.org/10.1093/sleep/zsaf118.

68. Porkka-Heiskanen, T., Strecker, R.E., Thakkar, M., Bjørkum, A.A., Greene, R.W., and McCarley, R.W. (1997). Adenosine: A mediator of the sleep-inducing effects of prolonged wakefulness. Science *276*, 1265–1268. https://doi.org/10.1126/science.276.5316.1265.

69. Peng, W., Wu, Z., Song, K., Zhang, S., Li, Y., and Xu, M. (2020). Regulation of sleep homeostasis mediator adenosine by basal forebrain glutamatergic neurons. Science *369*, eabb0556. https://doi.org/10.1126/science.abb0556.

70. Alfonsa, H., Burman, R.J., Brodersen, P.J.N., Newey, S.E., Mahfooz, K., Yamagata, T., Panayi, M.C., Bannerman, D.M., Vyazovskiy, V.V., and Akerman, C.J. (2023). Intracellular chloride regulation mediates local sleep pressure in the cortex. Nat. Neurosci. *26*, 64–78. https://doi.org/10.1038/s41593-022-01214-2.

71. Tian, Y., Kang, L., Ha, N.T., Deng, J., and Liu, D. (2025). Hydrogen peroxide in midbrain sleep neurons regulates sleep homeostasis. Cell Metab. *37*, 1442–1452.e7. https://doi.org/10.1016/j.cmet.2025.04.016.

72. Kempf, A., Song, S.M., Talbot, C.B., and Miesenböck, G. (2019). A potassium channel β-subunit couples mitochondrial electron transport to sleep. Nature *568*, 230–234. https://doi.org/10.1038/s41586-019-1034-5.

73. Yin, X., Zhang, Z., Zhou, R., Zuo, P., Sang, D., Zhou, S., Shi, B., Chen, L., Wu, C., Guo, Y., et al. (2025). Calcineurin governs baseline and homeostatic regulations of non-rapid eye movement sleep in mice. Proc. Natl. Acad. Sci. USA *122*, e2418317122. https://doi.org/10.1073/pnas.2418317122.

74. Heiss, J.E., Zhong, P., Lee, S.M., Yamanaka, A., and Kilduff, T.S. (2024). Distinct lateral hypothalamic CaMKIIalpha neuronal populations regulate wakefulness and locomotor activity. Proc. Natl. Acad. Sci. USA *121*, e2316150121. https://doi.org/10.1073/pnas.2316150121.

75. Mondino, A., Hambrecht-Wiedbusch, V.S., Li, D., York, A.K., Pal, D., González, J., Torterolo, P., Mashour, G.A., and Vanini, G. (2021). Glutamatergic neurons in the preoptic hypothalamus promote wakefulness, destabilize nrem sleep, suppress rem sleep, and regulate cortical dynamics. J. Neurosci. *41*, 3462–3478. https://doi.org/10.1523/JNEUROSCI.2718-20.2021.

76. Luo, Y.J., Ge, J., Chen, Z.K., Liu, Z.L., Lazarus, M., Qu, W.M., Huang, Z.L., and Li, Y.D. (2023). Ventral pallidal glutamatergic neurons regulate wakefulness and emotion through separated projections. iScience 26, 107385. https://doi.org/10.1016/j.isci.2023.107385.

77. Gerashchenko, D., Chou, T.C., Blanco-Centurion, C.A., Saper, C.B., and Shiromani, P.J. (2004). Effects of lesions of the histaminergic

tuberomammillary nucleus on spontaneous sleep in rats. Sleep *27*, 1275–1281. https://doi.org/10.1093/sleep/27.7.1275.

78. Blanco-Centurion, C., Gerashchenko, D., and Shiromani, P.J. (2007). Effects of saporin-induced lesions of three arousal populations on daily levels of sleep and wake. J. Neurosci. *27*, 14041–14048. https://doi.org/10.1523/JNEUROSCI.3217-07.2007.
79. Fuller, P., Sherman, D., Pedersen, N.P., Saper, C.B., and Lu, J. (2011). Reassessment of the structural basis of the ascending arousal system. J. Comp. Neurol. *519*, 933–956. https://doi.org/10.1002/cne.22559.
80. Renouard, L., Billwiller, F., Ogawa, K., Clément, O., Camargo, N., Abdelkarim, M., Gay, N., Scoté-Blachon, C., Touré, R., Libourel, P.A., et al. (2015). The supramammillary nucleus and the claustrum activate the cortex during REM sleep. Sci. Adv. *1*, e1400177. https://doi.org/10.1126/sciadv.1400177.
81. Gompf, H.S., Mathai, C., Fuller, P.M., Wood, D.A., Pedersen, N.P., Saper, C.B., and Lu, J. (2010). Locus ceruleus and anterior cingulate cortex sustain wakefulness in a novel environment. J. Neurosci. *30*, 14543–14551. https://doi.org/10.1523/JNEUROSCI.3037-10.2010.
82. Zecharia, A.Y., Yu, X., Götz, T., Ye, Z., Carr, D.R., Wulff, P., Bettler, B., Vyssotski, A.L., Brickley, S.G., Franks, N.P., et al. (2012). GABAergic inhibition of histaminergic neurons regulates active waking but not the sleep-wake switch or propofol-induced loss of consciousness. J. Neurosci. *32*, 13062–13075. https://doi.org/10.1523/JNEUROSCI.2931-12.2012.
83. Antila, H., Kwak, I., Choi, A., Pisciotti, A., Covarrubias, I., Baik, J., Eisch, A., Beier, K., Thomas, S., Weber, F., et al. (2022). A noradrenergic-hypothalamic neural substrate for stress-induced sleep disturbances. Proc. Natl. Acad. Sci. USA *119*, e2123528119. https://doi.org/10.1073/pnas.2123528119.
84. Voss, L.J., Young, B.J., Barnard, J.P., and Sleigh, J. (2005). Differential anaesthetic effects following microinjection of thiopentone and propofol into the pons of adult rats: A pilot study. Anaesth. Intensive Care *33*, 373–380. https://doi.org/10.1177/0310057X0503300313.
85. Devor, M., and Zalkind, V. (2001). Reversible analgesia, atonia, and loss of consciousness on bilateral intracerebral microinjection of pentobarbital. Pain *94*, 101–112. https://doi.org/10.1016/S0304-3959(01)00345-1.
86. Minert, A., Yatziv, S.L., and Devor, M. (2017). Location of the mesopontine neurons responsible for maintenance of anesthetic loss of consciousness. J. Neurosci. *37*, 9320–9331. https://doi.org/10.1523/JNEUROSCI.0544-17.2017.
87. Yatziv, S.L., Strumza, N., Minert, A., Baron, M., and Devor, M. (2021). A nodal point for brain-state transitions: the mesopontine tegmental anesthesia area (MPTA) in mice. Exp. Brain Res. *239*, 3255–3266. https://doi.org/10.1007/s00221-021-06204-7.
88. Vong, L.V., Ye, C., Zongfang, Y., Choi, B., Chua, S., Jr., and Lowell, B.B. (2011). Leptin Action on GABAergic Neurons Prevents Obesity and Reduces Inhibitory Tone to POMC Neurons. Neuron *71*, 142–154.
89. Foster, E., Wildner, H., Tudeau, L., Haueter, S., Ralvenius, W.T., Jegen, M., Johannssen, H., Hösli, L., Haenraets, K., Ghanem, A., et al. (2015). Targeted Ablation, Silencing, and Activation Establish Glycinergic Dorsal Horn Neurons as Key Components of a Spinal Gate for Pain and Itch. Neuron *85*, 1289–1304. https://doi.org/10.1016/j.neuron.2015.02.028.
90. Krashes, M.J., Koda, S., Ye, C.P., Rogan, S.C., Adams, A.C., Cusher, D.S., Maratos-Flier, E., Roth, B.L., and Lowell, B.B. (2011). Rapid, reversible activation of AgRP neurons drives feeding behavior in mice. J. Clin. Invest. *121*, 1424–1428. https://doi.org/10.1172/JCI46229.
91. Chen, T.W., Wardill, T.J., Sun, Y., Pulver, S.R., Renninger, S.L., Baohan, A., Schreiter, E.R., Kerr, R.A., Orger, M.B., Jayaraman, V., et al. (2013). Ultrasensitive fluorescent proteins for imaging neuronal activity. Nature *499*, 295–300. https://doi.org/10.1038/nature12354.
92. Yang, C.F., Chiang, M.C., Gray, D.C., Prabhakaran, M., Alvarado, M., Juntti, S.A., Unger, E.K., Wells, J.A., and Shah, N.M. (2013). Sexually dimorphic neurons in the ventromedial hypothalamus govern mating in both sexes and aggression in males. Cell *153*, 896–909. https://doi.org/10.1016/j.cell.2013.04.017.
93. Klugmann, M., Wymond Symes, C.W., Leichtlein, C.B., Klaussner, B.K., Dunning, J., Fong, D., Young, D., and During, M.J. (2005). AAV-mediated hippocampal expression of short and long Homer 1 proteins differentially affect cognition and seizure activity in adult rats. Mol. Cell. Neurosci. *28*, 347–360. https://doi.org/10.1016/j.mcn.2004.10.002.
94. Murray, A.J., Sauer, J.F., Riedel, G., McClure, C., Ansel, L., Cheyne, L., Bartos, M., Wisden, W., and Wulff, P. (2011). Parvalbumin-positive CA1 interneurons are required for spatial working but not for reference memory. Nat. Neurosci. *14*, 297–299. https://doi.org/10.1038/nn.2751.
95. Anisimov, V.N., Herbst, J.A., Abramchuk, A.N., Latanov, A.V., Hahnloser, R.H.R., and Vyssotski, A.L. (2014). Reconstruction of vocal interactions in a group of small songbirds. Nat. Methods *11*, 1135–1137. https://doi.org/10.1038/nmeth.3114.
96. Alexander, G.M.G.M., Rogan, S.C.S.C., Abbas, A.I.A.I., Armbruster, B.N.B.N., Pei, Y., Allen, J.A.J.A., Nonneman, R.J.R.J., Hartmann, J., Moy, S.S.S.S., Nicolelis, M.A.M.A., et al. (2009). Remote control of neuronal activity in transgenic mice expressing evolved G protein-coupled receptors. Neuron *63*, 27–39. https://doi.org/10.1016/j.neuron.2009.06.014.
97. Biever, A., Puighermanal, E., Nishi, A., David, A., Panciatici, C., Longueville, S., Xirodimas, D., Gangarossa, G., Meyuhas, O., Hervé, D., et al. (2015). PKA-dependent phosphorylation of ribosomal protein S6 does not correlate with translation efficiency in striatonigral and striatopallidal medium-sized spiny neurons. J. Neurosci. *35*, 4113–4130. https://doi.org/10.1523/JNEUROSCI.3288-14.2015.
98. Chang, J.W., Arnold, M.M., Rozenbaum, A., Caputo, A., Schweizer, F.E., Huynh, M., Mathern, G.W., Sarafian, T.A., and Watson, J.B. (2012). Synaptoneurosome micromethod for fractionation of mouse and human brain, and primary neuronal cultures. J. Neurosci. Methods *211*, 289–295. https://doi.org/10.1016/j.jneumeth.2012.09.005.
99. Yotova, A.Y., Li, L.L., O'Leary, A., Tegeder, I., Reif, A., Courtney, M.J., Slattery, D.A., and Freudenberg, F. (2024). Synaptic proteome perturbations after maternal immune activation: Identification of embryonic and adult hippocampal changes. Brain Behav. Immun. *121*, 351–364. https://doi.org/10.1016/j.bbi.2024.07.040.
100. Li, L.L., Melero-Fernandez de Mera, R.M.M.F., Chen, J., Ba, W., Kasri, N.N., Zhang, M., and Courtney, M.J. (2015). Unexpected heterodivalent recruitment of NOS1AP to nNOS reveals multiple sites for pharmacological intervention in neuronal disease models. J. Neurosci. *35*, 7349–7364. https://doi.org/10.1523/JNEUROSCI.0037-15.2015.
101. Schneider, C.A., Rasband, W.S., and Eliceiri, K.W. (2012). NIH Image to ImageJ: 25 years of image analysis. Nat. Methods *9*, 671–675. https://doi.org/10.1038/nmeth.2089.

STAR★METHODS

KEY RESOURCES TABLE

REAGENT or RESOURCE	SOURCE	IDENTIFIER
Antibodies		
Mouse anti-PSD95	UC Davis/NIH NeuroMab Facility	Cat# 75-028; RRID:AB _2292909
Mouse anti-GluA1	UC Davis/NIH NeuroMab Facility	Cat# N355/1; RRID: AB_2877405
Mouse anti-GluN1	Biolegend	RRID: AB_2801158
Mouse anti-β-actin	Genescript	RRID: AB_1968817
Rabbit anti-PKAc alpha	Invitrogen	RRID: AB_2170037
Rabbit anti-CaMKII (pan)	CST	RRID: AB_10545451
Rabbit anti-Phospho-CaMKII (Thr286)	CST	RRID: AB_2713889
Rabbit anti-Phospho-PKA C (Thr197)	CST	RRID: AB_2300165
Rabbit anti-Phospho-AMPA Receptor 1 (GluA1) (Ser831) (A502P)	CST	RRID: AB_2799873
Rabbit	CST	RRID: AB_10860773
Rabbit anti-Glutamate Receptor 2 & 3	Chemicon	RRID: AB_90710
Goat anti-mouse anti-rabbit-HRP	SCBT	RRID: AB_631746
rat monoclonal mCherry	Thermo Fisher Scientific	Cat# M11217; RRID: AB_2536611
chicken polyclonal GFP	Abcam	Cat# ab13970; RRID: AB_300798
Alexa Fluor 488 goat anti-rabbit	Invitrogen	Cat# A11008; RRID: AB_143165
Alexa Fluor 488 goat anti-mouse	Invitrogen	Cat# A11001; RRID: AB_2534069
Alexa Fluor 594 goat anti-rabbit	Invitrogen	Cat# A11037; RRID: AB_2534095
Alexa Fluor 594 goat anti-mouse	Invitrogen	Cat# A11005; RRID: AB_2534073
Alexa Fluor 594 goat anti-rat	Invitrogen	Cat# A11007; RRID: AB_10561522
Chemicals, peptides, and recombinant proteins		
clozapine-N-oxide	Sigma-Aldrich	C0832
Hoechst 33342	Thermo Fisher Scientific	H3507
Experimental models: Organisms/strains		
Mouse: *Vglut2-ires-Cre* (*Slc17a6*$^{tm2(cre)Lowl}$/*J*)	Jackson Lab	JAX Stock 016963
Mouse: *Vgat-ires-Cre* (*Slc32a1*$^{tm2(cre)Lowl}$/*J*)	Jackson Lab	JAX Stock 016962
Mouse: *GlyT2-Cre* (*Tg(Slc6a5-Cre)1Uze*)	Jackson Lab	JAX Stock 038515
Recombinant DNA		
Adenovirus helper plasmid *pFΔ6*	Donated by M Klugmann	NA
AAV helper plasmid *pH21* (AAV1)	Donated by M Klugmann	NA
AAV helper plasmid pRVI(AAV2)	Donated by M Klugmann	NA
pAAV-hSyn-DIO-hM3Dq-mCherry	Gift from Bryan L. Roth	Addgene plasmid 44361
pAAV-hSyn-DIO-hM4D(Gi)-mCherry	Gift from Bryan L. Roth	Addgene plasmid 44362
pAAV-hSyn-DIO-GCaMP6s	Addgene	Addgene plasmid 184284
pGP-CMV-GCaMP6s	Addgene	Addgene plasmid 40753
pAAV-EF1α-DIO-taCASP3-TEV	Gift from Nirao Shah	Addgene plasmid 45580
Software and algorithms		
Spike 2	Cambridge Electronic Design Limited	https://ced.co.uk/products/spkovin
Matlab	MathWorks	https://uk.mathworks.com/
Fiji	Fiji	https://fiji.sc/

EXPERIMENTAL MODEL AND STUDY PARTICIPANT DETAILS

Mice

All procedures were approved by the Animal Welfare Ethical Review Body at Imperial College London. Experiments were performed in accordance with the UK Home Office Animal Procedures Act (1986). *Vglut2-ires-Cre* mice (*Slc17a6*$^{tm2(cre)Lowl}$/*J*) and *Vgat-ires-Cre* mice (*Slc32a1*$^{tm2(cre)Lowl}$/*J*) were kindly provided by B.B. Lowell (JAX lab stock 016963 and JAX lab stock 016962).[88] *GlyT2-Cre* mice (*Tg(Slc6a5-Cre)1Uze*) were generated as described.[89] Mice were housed at constant temperature (22 ± 1 °C) and humidity and a reversed 12 h light-dark circadian cycle. Food and water were available *ad libitum*. Both male and female heterozygous mice 10-12 weeks of age at the start of experimental procedures were used in all experiments.

METHOD DETAILS

Viral constructs and preparation

Cre-inducible recombinant AAV vectors carrying transgenes encoding chemogenetic receptors (*pAAV-DIO-hM3Dq-mCherry* and *pAAV- DIO-hM4Di-mCherry*) were gifts from Bryan L. Roth (Addgene plasmids 44361 and 44362).[90] *pAAV-DIO-GFP* was a gift from Edward Boyden (Addgene plasmid 28304). For Ca^{2+} photometry experiments, plasmid *pAAV-DIO-GCaMP6s* (Addgene plasmid 184284) was generated by inserting the *GCaMP6s* open reading frame from *pGP-CMV-GCaMP6s* (Addgene plasmid 40753, gift of Douglas Kim)[91] into the *pAAV-DIO-hM3Dq-mCherry* backbone, as we described previously.[65] For the caspase lesions, *pAAV-EF1α-DIO-taCASP3-TEV* was a gift from Nirao Shah (Addgene plasmid 45580).[92] All vectors were packed into AAV capsids in-house (mixed 1:1 ratio of AAV1 and AAV2 capsids proteins with AAV2 inverted terminal repeats) as described previously.[93,94] Aliquots of virus were stored at -80 °C before stereotaxic injection.

Stereotaxic surgery

Mice were anesthetized with isoflurane (induced at 4% and maintained at 1.5%-2.5%) in oxygen (vol/vol) and positioned on a stereotaxic frame (Angle Two, Leica Microsystems, Milton Keynes, Buckinghamshire, UK). A heat pad was used during the surgery to prevent heat loss (ThermoStar, RWD Life Sciences, China). A digital mouse-brain atlas was linked to the injection frame to guide to the desired brain regions. The following coordinates were used for PnO: AP = -4.4 mm; ML = -0.8 mm; DV = 4.2 mm. The virus (0.2 – 0.3 μl total volume depending on the viral titer) was injected through a stainless steel 33-gauge/15-mm/PST3 internal cannula (Hamilton) attached to a 10 μl Hamilton syringe, at a rate of 0.1 μl min^{-1}. After infusion, the cannula was left at the injection site for 5 min and then slowly withdrawn.

For photometry recordings, following AAV injection, a mono-fiber optical cannula (200 μm; Doric Lenses Inc., Quebec, Canada) was placed 100 μm above the PnO and fixed with dental cement. We conducted post-mortem analysis to verify the viral injection sites and to evaluate the placement of the fiber optic. Only mice with appropriate viral expression pattern and fiber/cannula implantation were included in this study.

EEG and EMG recording and scoring of sleep-wake states

Non-tethered EEG and EMG recordings were captured using Neurologger 2A devices at a sampling rate of 200Hz as described previously.[95] Mice were implanted with three miniature screw electrodes (–1.5 mm Bregma, +1.5 mm midline, first recording electrode; -+1.5 mm Bregma, –1.5 mm midline, second recording electrode; –1 mm Lambda, 0 mm midline, reference electrode) with two EMG wires inserted in the dorsal neck muscles (AS634, Cooner Wire, CA). The EEG-EMG device was fixed to the skull with Orthodontic Resin powder and Orthodontic resin liquid (Tocdental, UK). All mice were allowed 3-4 weeks for recovery in their home cages. Collected data was downloaded and waveforms visualized using Spike2 software (Cambridge Electronic Design, Cambridge, UK). The EEG signals were high-pass filtered (0.5 Hz, -3dB, an FFT size of 512 sample was used as the designated time window) using a digital filter. The EMG signals were band-pass filtered between 5-45 Hz (-3dB). Power in the delta (0.5-4 Hz), theta (6-10 Hz) bands and theta to delta band ratios were calculated, along with the root mean square (RMS) value of the EMG signal (averaged over a bin size of 5 s). These data were used to define the vigilance states of WAKE, NREMS and REMS by an automatic script. Each vigilance state was subsequently screened and confirmed manually. The peak frequency during NREMS epochs were analyzed using Fourier transform power spectra to average power spectra over blocks of time.

For chemogenetic experiments,[96] clozapine-N-oxide (C0832, Sigma-Aldrich, dissolved in saline, 0.3 mg/kg) or saline was injected *i.p.*, and the vigilance states were recorded. Mice were split into random groups that received either saline or CNO injection. After conducting preliminary experiments, for the *hM3Dq-mCherry-receptor*-expressing mice, CNO or saline were injected during the "lights off" active phase.

Sleep deprivation

Sleep deprivation was performed at the start of "lights on" period (zeitgeber time 0, ZT0) when sleep pressure is the highest. Animals were sleep deprived for 5 h by introducing novel objects (mice were not touched directly to minimize the level of stress). Mice were then returned to their home cages for RS for 19 h. In total, sleep-wake states were recorded for 24 h for each mouse. RS was normalized to the corresponding baseline sleep of each mouse prior to comparison. For western blot experiments, PnO and cerebellum were micro-dissected and collected at ZT5 for control (undisturbed sleep) and SD groups. Tissues in the RS group were collected

at ZT6 after 1 h of RS. Patch-clamp experiments were performed at ZT6. Control animals underwent undisturbed sleep and RS animals were allowed 1 h of RS following 5 h of sleep deprivation.

Immunohistochemistry

Mice were deeply anesthetized with an overdose of pentobarbital (100 mg/kg body weight; i.p.) and transcardially perfused with 4% paraformaldehyde (Thermo Fisher Scientific, Inc, Massachusetts, United States) in phosphate buffered saline (PBS, pH 7.4, Sigma-Aldrich). After post-fixation overnight, the mouse brain was preserved in 30% sucrose/PBS for 2 days. 60-μm-thick coronal sections were sliced using a Leica SM 2010R microtome. Free-floating sections were washed in PBS three times for 5 min, permeabilized in PBS plus 0.4% Triton X-100 for 15 min and blocked by incubation in PBS plus 5% normal goat serum (NGS) (Vector), 0.2% Triton X-100 for 1 hour. Sections were incubated with primary antibody diluted in PBS plus 2% NGS overnight at 4°C in a shaker. Incubated slices were then washed three times in PBS for 10 min and incubated for 2 h with secondary antibody (Molecular Probes) in PBS and subsequently washed three times in PBS for 10 min (all at room temperature). Before mounting, slices were incubated with Hoechst 33342 (Thermo Fisher Scientific, Inc) for 15 min followed by rinsing with PBS. Finally, slices were mounted on slides, embedded in Dako mounting medium (Agilent Technologies, California, United States) and imaged using an inverted wide-field microscope (Zeiss Axio Observer) or a Leica SP5 MP confocal microscope (Facility for Imaging by Light Microscopy, FILM, Imperial College London).

Primary antibodies used were rat monoclonal mCherry (1:2000, Thermo Fisher Scientific, Inc); chicken polyclonal GFP (1:1000, Abcam, Cambridge, UK); Secondary antibodies were Alexa Fluor 488 goat anti-rabbit, Alexa Fluor 488 goat anti-mouse, Alexa Fluor 594 goat anti-rabbit, Alexa Fluor 594 goat anti-mouse (1:1000, Invitrogen Molecular Probes, UK).

Fiber photometry

A 473-nm diode-pumped solid-state blue laser (Shanghai Laser & Optics Century Co., Ltd) was used for GCaMP6s excitation. The laser light was passed through a single-source fluorescence cube (FMC_GFP_FC, Doric Lenses) through an optical fiber patch cord (Ø 200 μm, 0.22 numerical aperture, Doric Lenses). From the filter cube, a multimodal optical patch cord (Ø 200 μm, 0.37 numerical aperture) was attached to a ceramic optical fiber (Ø 200 μm, 0.37 numerical aperture) implanted into the mouse brain with a ceramic split mating sleeve ferrule (Thorlabs, New Jersey, United States). The GCaMP6 output was then filtered at 500–550 nm using a second dichroic mirror in the fluorescence cube and converted to voltage by an amplified photodiode (APD-FC, Doric Lenses). The photodiode signal was output to a lock-in amplifier (SR810, Stanford Research Systems) and the power of the laser was set to 80 μW at the fiber tip. The signal was then digitized using a CED 1401 Micro Box (Cambridge Electronic Design, Cambridge, UK) and recorded at 1 kHz using Spike2 software (Cambridge Electronic Design).

The photometry signal was aligned with the EEG and EMG recordings. For each experiment, the photometry signal F was normalized to the baseline signal using $\Delta F/F(t) = (F(t) - \text{median (F)})/\text{median } (F)$. We observed a decay of photometry signal at the beginning of some recordings. All the sessions were selected after the photometry signal became stable. We performed the recordings in 2–3 sessions per mouse, each session for 6 h. For the vigilance state transitions, several sessions were randomly chosen and analyzed.

Synaptoneurosomal preparation

PnO tissue from control, sleep-deprivation and RS groups were collected immediately after experiment. Tissue was rapidly frozen in Isopentane for subsequent synaptoneurosome extraction. Synaptoneurosomes were prepared using the filtration method[36] similar to that described previously.[97–99] Briefly, PnO tissue was gently homogenized with a Dounce tissue grinder (2 mL, Wilmad Labglass, United States) in ice cold synaptoneurosome buffer (in mM: NaCl 118, KCl 4.7, $MgSO_4$ 1.2, KH_2PO_4 1.53, Glucose 212.7, kynurenic acid 1, EGTA 0.5, HEPES 5, pH 7.4) supplemented with 1 mM DTT, 10 μg/mL protease inhibitors (aprotinin, leupeptin, and pepstatin A) and 0.1 mg/mL phenylmethanesulfonyl fluoride (PMSF). The homogenate was first centrifuged at 300 g, 4 °C, for 2min, to remove nuclei, larger cell fragments and unbroken cells. The supernatant was collected and filtered through buffer-equilibrated Mitex Membrane Filter paper (5.0 μm pore size, hydrophobic PTFE) (Merck Millipore, Massachusetts, United States). The flow-through was centrifuged at 14,000 g, 4 °C, for 4 min. Pellets containing synaptoneurosome were washed once with resuspension buffer (in mM: NaCl 118, KCl 4.7, $MgSO_4$ 1.2, EGTA 0.5, HEPES 5, pH 7.4) supplemented with 1 mM DTT, 10 μg/mL protease inhibitors (aprotinin, leupeptin, and pepstatin A), 0.1 mg/mL PMSF, and resuspended again in the same buffer. Protein concentration was determined using the Pierce™ 660nm Protein Assay Reagent (Thermo Fisher Scientific, Inc.). Samples were snap-frozen at -80°C. Samples were lysed in 1x Laemmli buffer (62.5 mM Tris-HCl; pH 6.8, 2% SDS, 10% glycerol, 2% beta-mercaptoethanol, and 0.02% bromophenol blue) and boiled 10 min at 95 °C for immunoblotting analyses.

Immunoblotting

Immunoblotting was performed similar to that previously.[100] Briefly, equal amounts of synaptoneurosome samples were loaded onto SDS-PAGE gels and transferred onto nitrocellulose membranes. Nitrocelluose membranes were blocked with 5% milk in TBS with 0.01% Tween for 1 h at room temperature followed by overnight incubation with primary antibodies at 4 °C. The primary and secondary antibodies used were as follows: anti-PSD95 mouse monoclonal antibody (0.5 μg/mL, K28/43, UC Davis/NIH NeuroMab Facility, RRID:AB_2292909), anti-GluA1 mouse monoclonal antibody (0.5 μg/mL, N355/1, UC Davis/NIH NeuroMab Facility, RRID:AB_2877405), anti-β-actin mouse monoclonal antibody (0.1 μg/mL, 2D1D10, Genescript, RRID:AB_1968817), anti-NMDAR1 monoclonal antibody (0.5 μg/mL, N308/48, Biolegend, RRID:AB_2801158), anti-PKAc alpha rabbit polyclonal antibody (0.5 μg/mL, PA1-30236, Invitrogen, RRID:AB_2170037), anti-CaMKII (pan) rabbit monoclonal antibody (1:1000, D11A10, CST,

RRID:AB_10545451), anti-Phospho-CaMKII (Thr286) rabbit monoclonal (1:1000, D21E4, CST, RRID:AB_2713889), anti-Phospho-PKA C (Thr197) rabbit polyclonal antibody (1:1000, #4781, CST, RRID:AB_2300165), anti-Phospho-AMPA Receptor 1 (GluA1) (Ser831) (A502P) rabbit monoclonal antibody (1:1000, CST, RRID:AB_2799873), anti-Phospho-AMPA Receptor 1 (GluA1) (Ser845) (D10G5) rabbit monoclonal antibody (1:1000, CST, RRID:AB_10860773), Anti-Glutamate Receptor 2 & 3 rabbit polyclonal (1:1000, Chemicon, RRID:AB_90710goat anti-rabbit-HRP (1:20000, #sc-2004, SCBT, RRID:AB_631746) and goat anti-mouse-HRP (1:20000, #sc-2005, SCBT, RRID:AB_631736).

Blots were developed using SuperSignal West Femto Maximum Sensitivity substrate (Thermo Fisher Scientific, Inc.) and pre-flashed X-ray films (Amersham Hyperfilm ECL, GE) were exposed to the blots. Images were quantified using ImageJ Gel Analyzer[101] (with background corrected profile analysis).

Acute slice electrophysiology recordings and single-cell RT-qPCR

Vgat-Cre mice were injected into the PnO area with *AAV-DIO-EGFP*. About a month later, mice underwent sleep deprivation or control experiences as described above (see section "sleep deprivation"). 5 h after sleep deprivation, when mice were in the RS period, mice were euthanized by cervical dislocation and subsequent decapitation. The brain was rapidly retrieved to be sliced and placed into cold oxygenated N-methyl-D-glucamine (NMDG) solution (in mM: NMDG 93, HCl 93, KCl 2.5, NaH_2PO_4 1.2, $NaHCO_3$ 30, HEPES 20, glucose 25, sodium ascorbate 5, thiourea 2, sodium pyruvate 3, $MgSO_4$ 10, $CaCl_2$ 0.5). Para-horizontal or coronal slices (thickness 220 μm) encompassing the PnO area were obtained using a vibrotome (Vibrating Microtome 7000 smz-2; Campden Instruments, Ltd.). Slices were incubated for 15 min in NMDG solution at 33°C with constant oxygenation and transferred to oxygenated standard aCSF (in mM: NaCl 120, KCl 3.5, NaH_2PO_4 1.25, $NaHCO_3$ 25, glucose 10, $MgCl_2$ 1, $CaCl_2$ 2) solution for at least 1 h at RT. Slices were transferred to a submersion recording chamber and were continuously perfused at a rate of 4–5 mL/min with fully oxygenated aCSF at room temperature. For whole-cell recording, patch pipettes at 4 – 6MΩ were pulled from borosilicate glass capillaries (1.5 mm OD, 0.86 mm ID, Harvard Apparatus, #GC150F-10) and filled with intracellular solution containing in mM: 128 $CsCH_3SO_3$, 2.8 NaCl,20 HEPES, 0.4 EGTA, 5 TEA-Cl, 2 Mg-ATP, 0.5 NaGTP (pH7.35, osmolality 285 mOsm). 0.1% Neurobiotin was included in the intracellular solutions to identify the cell position and morphology following recording. Recordings were performed using a Multiclamp 700B amplifier (Molecular Devices, California, United States). Access and input resistances were monitored throughout the experiments. The access resistance was typically 20 MΩ, and results we discarded if resistance changed by more than 20%.

GFP-positive neurons were visually identified and randomly selected. For AMPA and NMDA currents, a bipolar stimulus microelectrode (MX21AEW, FHC, ME, United States) was placed 100–200μm away caudally from the recording site. The intensity of stimulus (10 ms) was adjusted to evoke a measurable, evoked EPSC (eEPSC) in recording cells. AMPA and NMDA mixed currents were measured at a holding potential of +40mV. After obtaining at least 10 sweeps of stable mixed currents, the NMDA blocker D-AP5 (50 μM) was perfused in the bath solution for 15 min and AMPA currents were measured. NMDA currents were obtained by subtracting AMPA currents from mixed currents off-line. The mean peak amplitude of both currents was used for AMPA/NMDA ratio analysis. All recordings were made in the presence of Picrotoxin (100μM) to block $GABA_AR$-mediated currents. For immunohistochemistry following electrophysiological recordings, brain slices were postfixed in 4% paraformaldehyde overnight at 4 °C. Paraformaldehyde was then washed away three times for 15 min in PBS and slices were blocked and permeabilized in 10% NGS, 0.2% Triton X-100 in PBS (PBSTx) for 3 h while shaking. Primary anti-GFP antibody to trace viral distribution was diluted in 2% NGS, 0.2% PBSTx for 2 nights at 4°C while shaking. After four washes in 0.2% PBSTx for 30 min each, secondary antibody and an Alexa594-conjugated streptavidin (Invitrogen) was diluted in 2% NGS and 0.2% PBSTx overnight at 4 °C while shaking. After four washes of 15 min in PBS, slices were mounted on glass slides.

At the end of each recording, cytoplasm was aspirated into the patch pipette, and expelled into a PCR tube containing lysate buffer with DNase I solution. The single-cell RT-qPCR assays were performed using the Ambion Single-Cell to CT Kit (Invitrogen). Reverse transcription and complementary DNA pre-amplification were performed according to the kit protocol. Quantitative PCR was performed using the TaqMan Gene Expression Assay system (Applied Biosystems). The mouse TaqMan assay probes were designed by and purchased from Invitrogen (Thermo Fisher): *Vgat* (Mm00494138_m1); *GlyT2* (Mm01202538_m1); *Vglut2* (Mm00499876_m1); *Pvalb* (Mm00443100_m1); *Sst* (Mm00436671_m1); *Calb1* (Mm00499876_m1); *Calb2* (Ec06990451_m1).

QUANTIFICATION AND STATISTICAL ANALYSIS

Mice with an incorrect viral expression or fiber/cannula placement were excluded from the analysis. Data distribution was assumed to be normal, but this was not formally tested. Analyses were performed with GraphPad Prism 8 (GraphPad software) and MATLAB (Mathworks). Data are presented as means ± SEM. For analyzing sleep changes, we used either two-tailed *t*-test or paired *t*-test. Data from western blot were analyzed by one-way ANOVA followed by Tukey's multiple comparisons post hoc test. For electrophysiology, we used Welch's t-test. *P*-values are shown when they were <0.05.